Floquet-induced superfluidity with periodically modulated interactions of two-species hardcore bosons in a one-dimensional optical lattice

Tao Wang (汪涛),[1,2] Shijie Hu (胡时杰),[2,*] Sebastian Eggert,[2] Michael Fleischhauer,[2]
Axel Pelster,[2] and Xue-Feng Zhang (张学锋)[1]

[1]*Department of Physics, Chongqing University, Chongqing, 401331, China*
[2]*Physics Department and Research Center OPTIMAS, Technische Universität Kaiserslautern, 67663 Kaiserslautern, Germany*

(Received 20 June 2018; revised manuscript received 24 July 2019; accepted 31 January 2020; published 6 March 2020)

We consider two species of hard-core bosons with density-dependent hopping in a one-dimensional optical lattice, for which we propose experimental realizations using time-periodic driving. The quantum phase diagram for half-integer filling is determined by combining different advanced numerical simulations with analytic calculations. We find that a *reduction* of the density-dependent hopping induces a Mott-insulator to superfluid transition. For negative hopping, a gauge-dressed superfluid state is found where one species induces a gauge phase of the other species, which leads to a superfluid phase of gauge-paired particles. The corresponding experimental signatures are discussed.

DOI: 10.1103/PhysRevResearch.2.013275

I. INTRODUCTION

Recent developments for ultracold-atomic systems provide useful platforms for quantum simulations in a wide window of tunable parameters [1,2]. Interacting bosons in an optical lattice show a quantum phase transition from a superfluid (SF) to a Mott insulator (MI) [3,4], which has been experimentally shown by "time-of-flight" measurements [5] of the momentum distribution [6]. In a mixture of different species, the interaction strengths for both inter- and intraspecies scattering can be tuned via Feshbach resonances [7]. As a result, a large variety of interesting new phases have been predicted for spinor bosons [8–11], interacting multispecies bosons or fermions [12–16], and Bose-Fermi mixtures [17–19].

Recently, time-dependent and driven optical lattices have opened an era of exploring exotic dynamical quantum states [20–46]. For instance, assisted Raman tunneling and shaking were proposed to induce a density-dependent complex phase in the hopping elements, which may allow the experimental realization of anyonic physics [26–29]. On the other hand, a fast time-periodic modulation of the interaction [30,31] will lead to an effective hopping matrix element depending on the density difference [32–37], which gives rise to pair superfluidity in one dimension (1D) [32], while superfluidity is suppressed in higher dimensions [33]. Experimental realizations of time-periodic driving [37–46] demonstrate that signatures of interesting effective models can be observed before heating or decoherence destroys the so-called Floquet states.

In this article, we propose a realization of a density-dependent hopping model of two interacting bosonic species in 1D via time-periodic driving, which results in a rich and interesting quantum phase diagram. Using a combination of advanced numerical methods, we find that a reduction of the density-dependent hopping by driving, counterintuitively causes a MI to SF quantum phase transition. For larger driving, we obtain negative effective hopping, which gives rise to an exotic SF phase of gauge-dressed composite particles.

The paper is organized as follows: In Sec. II, we propose the realization schemes of two different time-periodically driven models of two-species hardcore bosons in experiments. Both models result in effective density-dependent hopping, which is derived in Sec. III using Floquet theory in the high-frequency expansion. The effective model at half-filling is analyzed in detail in Sec. IV, where we show interesting behavior induced by the external driving in the quantum phase diagram and discuss the physical implications. The conclusion and outlook are presented in Sec. V.

II. EXPERIMENTAL REALIZATIONS OF TIME-PERIODICALLY DRIVEN MODELS

In this section, we will provide two experimental proposals to realize a hard-core Bose-Hubbard model with two interacting species and occupation-dependent hopping, which is achieved by periodically driven cold atoms in an optical lattice in combination with Feshbach resonances.

Our starting point is an ultracold gas of bosons with two hyperfine states a and b in a deep 1D optical lattice,

$$V(x) = V_0 \sin^2(k_r x), \tag{1}$$

*Corresponding author: shijiehu201@gmail.com

with the lattice depth V_0, wave vector $k_r = 2\pi/\lambda_L$, and wavelength λ_L. In the single-band approximation, the Hamiltonian is given by hopping elements between neighboring sites,

$$\hat{H}_T = -\sum_l (J_a \hat{a}_l^\dagger \hat{a}_{l+1} + J_b \hat{b}_l^\dagger \hat{b}_{l+1} + \text{H.c.}), \tag{2}$$

where $\hat{a}_l$ ($\hat{b}_l$) and $\hat{a}_l^\dagger$ ($\hat{b}_l^\dagger$) are the annihilation and creation operators, J_a (J_b) is the hopping coefficient of atoms with hyperfine level a (b), and the site index l runs over the whole lattice. Obviously, $J_a = J_b = J$ because the hopping processes are independent of the hyperfine internal states of the atoms [9]. Hereafter, we choose $J = 1$ as a unit. As described in Ref. [16], it is possible to prepare the initial state with an equal occupation of a and b states, which is assumed in the following.

The depth of the optical lattice potential determines the amplitude of the on-site repulsive interaction between the ultracold atoms [9], which is independent of the hyperfine states unless we are close to a Feshbach resonance point. Therefore, increasing the lattice depth V_0 will generate large intra- and interspecies repulsive interactions independent of the hyperfine states,

$$\hat{H}_L = \frac{U_L}{2} \sum_l \left(\hat{n}_l^a + \hat{n}_l^b\right)\left(\hat{n}_l^a + \hat{n}_l^b - 1\right), \tag{3}$$

where $\hat{n}_l^a = \hat{a}_l^\dagger \hat{a}_l$ ($\hat{n}_l^b = \hat{b}_l^\dagger \hat{b}_l$) denote the particle-number operator of the species a (b), and $U_L \gg J$. To fulfill the hard-core constraint, the lattice depth V_0 must be chosen significantly larger than the recoil energy, $E_r = h^2/2m\lambda_L^2$, with atomic mass m and Planck constant h. We need $s = V_0/E_r \gtrsim 20$ or larger [4], while the hopping is approximately $J \sim 4E_r s^{3/4} \exp(-2\sqrt{s})/\sqrt{\pi}$ [47]. For ^{87}Rb, we therefore have $E_r/h \sim 3.5$ kHz in a 400 nm lattice, which gives $J/h \sim 17$ Hz.

Furthermore, we suggest to add a static magnetic field and tune its amplitude B to be very close to the Feshbach resonance point B_0, where two-species atoms form s-wave bound states [7,48]. On the side of the negative scattering length, an attractive interspecies interaction emerges, with an additional energy,

$$\hat{H}_F = -U_F \sum_l \hat{n}_l^a \hat{n}_l^b, \quad U_F > 0. \tag{4}$$

Here, U_F can be tuned to large magnitudes comparable to U_L, so it can compensate the interspecies interaction in Eq. (3) and result in a total finite repulsion $U = U_L - U_F$ between n_a and n_b, which is assumed to be of the order of J. Meanwhile, the intraspecies interaction is not close to resonance at this field, so that the large intraspecies repulsion U_L in the lattice still leads to the hard-core constraint, which means more than one atom from the *same* species is forbidden at the same lattice site. Taking ^{87}Rb atoms, for example, we can choose the magnetic field to be a little smaller than the interspecies Feshbach resonance point 1259.96 G and far away from the intraspecies ones, which are located at 685.43 G for $|F = 1, m_F = 1\rangle$ (a) and 661.43 G for $|F = 1, m_F = 0\rangle$ (b) [48].

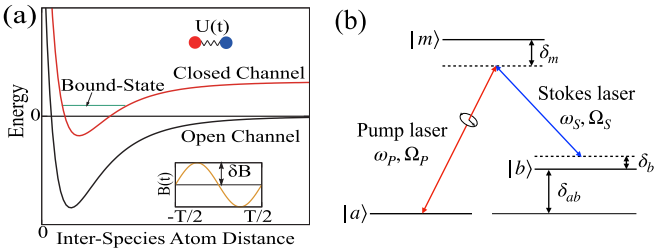

FIG. 1. (a) The realization of time-periodically modulated interspecies interaction by imposing a periodically modulated magnetic field (see inset) near the Feshbach resonance. (b) Schematic picture of the standard simulated Raman transition. An atom jumps from the hyperfine state a to the intermediate state m by absorbing a photon from a pump laser (red line, frequency ω_P, fast rotating linearly polarized, coupling strength Ω_P). Similarly, an atom jumps from m to b by emitting a photon from a Stokes laser (blue line, frequency ω_S, *linearly polarized*, coupling strength Ω_S) [49]. One realization of the pump laser is the output of a circularly polarized laser passing a 1/4 wave plate which is connected to a fast rotating mechanical motor (frequency ω sets several kHz).

A. Periodically modulated interspecies interaction

A straightforward, but technologically challenging time-periodic driving can be realized by an oscillating magnetic field $B(t) = \bar{B} + \delta B \cos(\omega t)$ near B_0, where $\bar{B}$ denotes the time-average strength of the magnetic field, δB represents the oscillation amplitude of the magnetic field, and ω stands for the oscillating frequency, as shown in Fig. 1(a). Thus, the relevant s-wave scattering length can be written as

$$a_s(t) = a_{bg}\left[1 - \frac{\Delta}{\bar{B} + \delta B \cos(\omega t) - B_0}\right], \tag{5}$$

where Δ is the width of the Feshbach resonance and a_{bg} represents the background scattering length, which is determined by the lattice depth. If we choose $\delta B \ll |\bar{B} - B_0|$, we can further perform a Taylor series expansion of $a_s(t)$ with respect to a small value of $\delta B/(\bar{B} - B_0)$ and get

$$a_s(t) = a_s^{(0)} + a_s^{(1)} \cos(\omega t) + \mathcal{O}\left[\left(\frac{\delta B}{\bar{B} - B_0}\right)^2\right], \tag{6}$$

where the coefficients of the leading orders are $a_s^{(0)} = a_{bg}[1 - \Delta/(\bar{B} - B_0)]$ and $a_s^{(1)} = a_{bg}\Delta\delta B/(\bar{B} - B_0)$. Note that a pure cosine oscillation of a_s is, in principle, also possible for larger amplitude δB if the waveform of the magnetic field is adjusted correspondingly. The interspecies interaction energy $U(t)$ is proportional to the related scattering length, which means $U(t) = \bar{U} + \delta U \cos(\omega t)$, where the time-average energy $\bar{U}$ is proportional to $a_s^{(0)}$ and the oscillation amplitude δU is proportional to $a_s^{(1)}$ if we neglect higher-order terms. In this case, the system can be described by the following Hamiltonian:

$$\hat{H}_1(t) = -J \sum_l (\hat{a}_l^\dagger \hat{a}_{l+1} + \hat{b}_l^\dagger \hat{b}_{l+1} + \text{H.c.}) + U(t) \sum_l \hat{n}_l^a \hat{n}_l^b. \tag{7}$$

B. Periodically modulated Rabi oscillation

The proposed fast oscillating magnetic fields are possible but challenging, so an alternative experimental realization in a static magnetic field is useful. To this end, we propose to gradually switch on a pair of Raman laser beams, which are coupled to the atomic cloud with the frequency difference $\delta\omega_R$. An atomic transition from the hyperfine state a to b by a two-photon emission absorption has the standard Λ form [49], shown in Fig. 1(b). One pump laser initiates that atoms jump from the hyperfine state $|a\rangle$ to the intermediate state $|m\rangle$ by absorbing a photon with frequency ω_P and coupling strength Ω_P, while the other Stokes laser triggers atoms to jump from $|m\rangle$ to $|b\rangle$ by emitting a photon with frequency ω_S and coupling strength Ω_S [49]. With this, we obtain the Hamiltonian for the Rabi transition,

$$\hat{H}_\Omega = J_\Omega \sum_l (\hat{a}_l^\dagger \hat{b}_l + \text{H.c.}), \tag{8}$$

where we neglect the small shift of the chemical potential δ between two hyperfine levels.

In order to produce a time-periodic oscillating Rabi coupling strength, we let the polarization direction of the pump laser circulate in time, e.g., $E_x = A\cos(\omega t)$ and $E_z = A\sin(\omega t)$, with the amplitude of the polarization A.

For realization, a circularly polarized pump laser may pass through a 1/4 wave plate to get a linearly polarized laser beam as output, the polarization direction of which is 45° shifted to the optical axis of the wave plate. Sequentially, the wave plate is connected to a mechanical motor with rotating frequency ω in the kHz range, which is much lower than the laser frequency of several hundreds of THz (10^{12} Hz). Therefore, the polarization of the pump laser is also rotating and effectively provides a time-modulated Rabi coupling. In order to avoid coupling to other magnetic sublevels when the linear polarization is rotated, we assume a sufficiently strong Zeeman splitting. Therefore, assuming $d_z = 0$, we get

$$\Omega_P = \langle m|Ad_x\cos(\omega t)|a\rangle = \Omega_P^0\cos(\omega t), \tag{9}$$

with $\Omega_P^0 = \langle m|Ad_x|a\rangle$. As a result, the effective Rabi frequency turns out to be time periodic,

$$J_\Omega(t) = J_\Omega^0\cos(\omega t), \tag{10}$$

with the amplitude $J_\Omega^0 = \Omega_P^0\Omega_S/\delta_m$. We can use, for instance, an acousto-optic modulator (AOM) to change both the amplitude and the polarization of the pump laser [50,51]. Thus, the full Hamiltonian reads

$$\hat{H}_2(t) = -J\sum_l (\hat{a}_l^\dagger \hat{a}_{l+1} + \hat{b}_l^\dagger \hat{b}_{l+1} + \text{H.c.}) + \hat{H}_{\bar{U}} + J_\Omega(t)\sum_l (\hat{a}_l^\dagger \hat{b}_l + \text{H.c.}), \tag{11}$$

where the time-independent on-site repulsion is $\hat{H}_{\bar{U}} = \bar{U}\sum_l \hat{n}_l^a\hat{n}_l^b$.

The rotating frequency of the time-periodic driving for two cases must be much larger than J and U, but not too large to avoid "photon-assisted hopping" between different energy bands of the optical lattice. In the following discussion of possible realizations, we therefore assume a rotating frequency ω of the order of kHz, which will also be the order of magnitude of the driving amplitude.

III. EFFECTIVE HAMILTONIAN

For a system with time-periodic Hamiltonian $\hat{H}(t) = \hat{H}(t+T)$ with period T, the steady state can be described by Floquet theory, which is equivalent to a time-independent eigenvalue problem. It is possible to derive an effective static Hamiltonian using a high-frequency expansion [32–37]. We will now demonstrate this procedure explicitly for the proposed setups from the previous setups, also including relatively large energy scales δU and J_Ω^0, which may be of the same order as ω. Therefore, we need to apply a rotation $\hat{V}$ at the preliminary step in order to eliminate these extra terms by moving them to the phases of the respective hopping terms [35],

$$\hat{H}_r(t) = \hat{V}^\dagger[\hat{H}(t) - i\hbar\partial/\partial t]\hat{V}. \tag{12}$$

In the following, we will calculate the effective Hamiltonian for both driven cases separately; the so-called kick operator is calculated in Appendix A.

A. Periodically modulated interspecies interaction

For the periodically modulated interspecies Hamiltonian (7), the rotation operator is given by $\hat{V}(t) = \exp(-i\tilde{K}_U\sum_l \hat{n}_l^a\hat{n}_l^b)$ with dimensionless modulation strengths $\tilde{K}_U = K_U\sin(\omega t)$ and $K_U = \delta U/\hbar\omega$. With this, the rotated Hamiltonian becomes

$$\hat{H}_r = -J\sum_l \left(\hat{a}_l^\dagger e^{i\tilde{K}_U(\hat{n}_l^b - \hat{n}_{l+1}^b)}\hat{a}_{l+1} + \hat{b}_l^\dagger e^{i\tilde{K}_U(\hat{n}_l^a - \hat{n}_{l+1}^a)}\hat{b}_{l+1} + \text{H.c.}\right) + \hat{H}_{\bar{U}}. \tag{13}$$

Here, $\hat{H}_r$ is again time periodic and can thus be expanded in a Fourier series $\hat{H}_r = \sum_{n=-\infty}^{\infty}\hat{H}_r^{(n)}e^{in\omega t}$, with

$$\hat{H}_r^{(n)} = -J\sum_l \left\{\hat{a}_l^\dagger \mathcal{J}_n\left[K_U\left(\hat{n}_l^b - \hat{n}_{l+1}^b\right)\right]\hat{a}_{l+1} + \hat{b}_l^\dagger \mathcal{J}_n\left[K_U\left(\hat{n}_l^a - \hat{n}_{l+1}^a\right)\right]\hat{b}_{l+1} + \text{H.c.}\right\} + \delta_{n,0}\hat{H}_{\bar{U}}, \tag{14}$$

where $\mathcal{J}_n$ denotes the nth-order Bessel function of the first kind.

Now we can calculate the effective Hamiltonian order by order [35]. The zeroth-order effective Hamiltonian is

$$\hat{H}_e^{(0)} = \hat{H}_r^{(0)}, \tag{15}$$

and the first-order effective Hamiltonian vanishes, i.e.,

$$\hat{H}_e^{(1)} = \sum_{n=1}^{+\infty}\frac{1}{n\hbar\omega}\left[\hat{H}_r^{(n)}, \hat{H}_r^{(-n)}\right] = 0, \tag{16}$$

where we use the property $\hat{H}_r^{(n)} = (-1)^n\hat{H}_r^{(-n)}$. All second-order corrections consist of many terms, which are accompanied by the prefactor $(J/\hbar\omega)^2$ and are not listed here. In the limit $J/\hbar\omega \ll 1$, all higher-order corrections to the zeroth-order effective Hamiltonian are small.

B. Periodically modulated Rabi oscillation

We now deal with the Hamiltonian (11), which describes a periodically modulated Rabi oscillation. In the case of $\delta U = 0$ and $U = \bar{U}$, the rotation transformation is given by $\hat{V}(t) = \exp[-i\tilde{K}_\Omega(\hat{a}_l^\dagger \hat{b}_l + \text{H.c.})]$ with dimensionless modulation strengths $\tilde{K}_\Omega = K_\Omega \sin(\omega t)$ and $K_\Omega = J_\Omega^0/\hbar\omega$, so we get

$$\begin{aligned}\hat{V}^\dagger \hat{a}_l^\dagger \hat{V} &= \cos\tilde{K}_\Omega \hat{a}_l^\dagger + i \sin\tilde{K}_\Omega \hat{b}_l^\dagger \big(1 - 2\hat{n}_l^a\big),\\ \hat{V}^\dagger \hat{a}_l \hat{V} &= \cos\tilde{K}_\Omega \hat{a}_l - i \sin\tilde{K}_\Omega \hat{b}_l \big(1 - 2\hat{n}_l^a\big).\end{aligned} \tag{17}$$

Thus, the rotated Hamiltonian results in

$$\hat{H}_r(t) = \hat{V}^\dagger(\hat{H} - i\hbar\partial/\partial t)\hat{V} = \hat{H}_r^T(t) + \hat{H}_{\bar{U}}, \tag{18}$$

where we have

$$\begin{aligned}\hat{H}_r^T(t) = -J \sum_l \Big\{ &\cos\big[2\tilde{K}_\Omega\big(\hat{n}_l^b - \hat{n}_{l+1}^b\big)\big]\hat{a}_l^\dagger \hat{a}_{l+1}\\ &+ \cos\big[2\tilde{K}_\Omega\big(\hat{n}_l^a - \hat{n}_{l+1}^a\big)\big]\hat{b}_l^\dagger \hat{b}_{l+1}\\ &- i\sin\big[2\tilde{K}_\Omega\big(\hat{n}_l^a - \hat{n}_{l+1}^b\big)\big]\hat{b}_l^\dagger \hat{a}_{l+1}\\ &- i\sin\big[2\tilde{K}_\Omega\big(\hat{n}_l^b - \hat{n}_{l+1}^a\big)\big]\hat{a}_l^\dagger \hat{b}_{l+1} + \text{H.c.}\Big\}.\end{aligned} \tag{19}$$

Also, here $\hat{H}_r(t)$ is time periodic and can be expanded in a Fourier series, namely, $\hat{H}_r(t) = \sum_{n=-\infty}^{+\infty} \hat{H}_r^{(n)} e^{in\omega t}$, with

$$\begin{aligned}\hat{H}_r^{(2m)} = -J \sum_l \Big\{ &\mathcal{J}_{2m}\big[2K_\Omega\big(\hat{n}_l^b - \hat{n}_{l+1}^b\big)\big]\hat{a}_l^\dagger \hat{a}_{l+1}\\ &+ \mathcal{J}_{2m}\big[2K_\Omega\big(\hat{n}_l^a - \hat{n}_{l+1}^a\big)\big]\hat{b}_l^\dagger \hat{b}_{l+1}\\ &+ \text{H.c.}\Big\} + \delta_{2m,0}\hat{H}_{\bar{U}},\\ \hat{H}_r^{(2m+1)} = J \sum_l \Big\{ &\mathcal{J}_{2m+1}\big[2K_\Omega\big(\hat{n}_l^a - \hat{n}_{l+1}^b\big)\big]\hat{b}_l^\dagger \hat{a}_{l+1}\\ &+ \mathcal{J}_{2m+1}\big[2K_\Omega\big(\hat{n}_l^b - \hat{n}_{l+1}^a\big)\big]\hat{a}_l^\dagger \hat{b}_{l+1} + \text{H.c.}\Big\}\end{aligned} \tag{20}$$

for even and odd orders, respectively, in which $\mathcal{J}_n$ is the nth-order Bessel function of the first kind.

Similar to the first case, we obtain the high-frequency expansion of the effective Hamiltonian [35] in the rotating frame, namely, $\hat{H}_e = \sum_{n=0}^{+\infty} \hat{H}_e^{(n)}$. The zeroth-order effective Hamiltonian is $\hat{H}_e^{(0)} = \hat{H}_r^{(0)}$ and the first order in $J/\hbar\omega$ also vanishes. The second-order correction consists of many terms proportional to $(J/\hbar\omega)^2$ and will again be ignored in the limit $J/\hbar\omega \ll 1$.

C. General effective model

In conclusion, in both cases, a time-independent effective Hamiltonian with density-dependent hopping can be reached by adiabatically increasing the driving amplitude,

$$\hat{H}_e^{(0)} = \sum_{l=1}^{L} \big(-\hat{J}_l^a \hat{a}_l^\dagger \hat{a}_{l+1} - \hat{J}_l^b \hat{b}_l^\dagger \hat{b}_{l+1} + \bar{U}\hat{n}_l^a \hat{n}_l^b\big), \tag{21}$$

where the hoppings $\hat{J}_l^{a/b}$ are now operators depending on the local densities of the opposite species,

$$\hat{J}_l^b = J\,\mathcal{J}_0\big[K\big(\hat{n}_l^a - \hat{n}_{l+1}^a\big)\big], \tag{22}$$

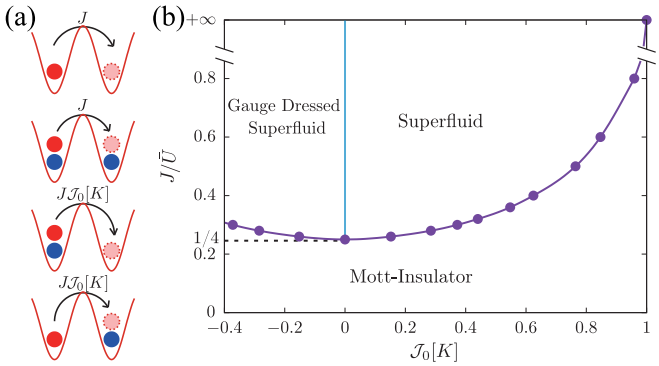

FIG. 2. (a) Hopping processes of one species a (red filled circle) in the effective model in Eq. (21). The other species b is denoted by blue filled circles. Hopping between two neighboring single occupied or double/empty sites is suppressed by $\mathcal{J}_0[K]$. (b) Quantum phase diagram of the effective model in Eq. (21) at half filling.

with matrix elements

$$\begin{cases} J & \text{for } n_l^a - n_{l+1}^a = 0\\ J\mathcal{J}_0[K] & \text{for } |n_l^a - n_{l+1}^a| = 1,\end{cases} \tag{23}$$

and analogously for $\hat{J}_l^a$. Here, $\mathcal{J}_0[K]$ denotes the zeroth-order Bessel function of the first kind and the dimensionless driving amplitude $K = \delta U/\hbar\omega$ or—*alternatively*—$K = 2J_\Omega^0/\hbar\omega$ gives the modulation strength in units of $\hbar\omega$. As illustrated in Fig. 2(a), the effect of driving is therefore to suppress hopping of hard-core type-a bosons by $\mathcal{J}_0[K]$ if the occupation of type-b bosons is different, and vice versa. The suppression decreases with increasing driving K from $\mathcal{J}_0[0] = 1$ to the negative minimum value of $\mathcal{J}_0[3.8717] \approx -0.4024$.

Further tuning parameters of the model are possible, e.g., by an asymmetry in the pulse sequence [39], which makes this setup an interesting general platform. In this article, we will focus on the phase diagram of the model (21) at half filling, $\langle\hat{n}_l^a\rangle = \langle\hat{n}_l^b\rangle = 1/2$. In this case, the undriven system $\mathcal{J}_0[0] = 1$ is known to be in the Mott state for any $\bar{U} > 0$ without a quantum phase transition [52]. However, as we will see below, the selective *reduction* of hopping elements by driving will destroy the MI state.

IV. QUANTUM PHASE DIAGRAM AT HALF FILLING

A. Integrable point

An interesting point is reached at the zeros of the Bessel function since for $\mathcal{J}_0[K] = 0$ the hopping between neighboring double occupied and empty sites is not possible in this case, as shown in Fig. 2(a). Because the Hamiltonian no longer distinguishes between double occupied and empty sites, we can denote both of them with pseudospin up $|\uparrow\rangle$ (for $n_l^a = n_l^b$). Likewise, hopping between neighboring single occupied sites is forbidden regardless of whether they are type a or b, so both can be denoted with pseudospin down $|\downarrow\rangle$ (for $n_l^a \neq n_l^b$). The corresponding total occupation numbers for the four different possible local states (a, b, double, empty) are all conserved and the resulting Hamiltonian for half filling is

expressed exactly as

$$\hat{H}_e^{(0)} = \sum_{l=1}^{L} \left[-J(\hat{S}_l^+ \hat{S}_{l+1}^- + \text{H.c.}) + \frac{\bar{U}}{2}\left(\hat{S}_l^z + 1/2\right) \right], \quad (24)$$

where $\hat{S}_l^{+/-}$ and $\hat{S}_l^z$ represent the respective pseudospin-1/2 operators. There is a macroscopic degeneracy 2^L increasing with the number of sites L, since each pseudospin state represents two different but equivalent local states for each site. The xy model in Eq. (24) is exactly solvable, where $\bar{U}$ provides a Zeeman splitting between $|\uparrow\rangle$ and $|\downarrow\rangle$. For $\bar{U} > 4J$, the system is saturated with only single occupied sites and a finite charge gap corresponding to the MI phase. When $\bar{U} \leqslant 4J$, the ground state is in a gapless xy phase *without* the SF response, indicated by a blue vertical line in Fig. 2(b). Details of the solution and correlations at the degenerate line are discussed in Appendix B.

B. Floquet-induced normal superfluidity

To obtain the full quantum phase diagram at half filling, we now use a combination of three independent advanced numerical simulation methods. The density matrix renormalization group (DMRG) method [53–56] is used to measure the properties of finite-size chains, such as the charge gap Δ_c, the superfluid density ρ_s, and correlation functions using up to $M = 4096$ states. With the further development of the DMRG to infinite systems (iDMRG) [57–59], we can moreover determine the fidelity susceptibility χ_F and the entanglement entropy $\mathcal{S}$ directly in the thermodynamic limit. Last but not least, the stochastic series expansion algorithm of the quantum Monte Carlo (QMC) method with parallel tempering [60–62] is used to calculate the compressibility κ close to the zero-temperature limit.

As shown in Fig. 3(a) for $J = 0.4\bar{U}$, we now observe signatures of a quantum phase transition at half filling as a function of the effective hopping $\mathcal{J}_0[K]$, which is reduced by the driving amplitude K. Because the phase transition is of the Berezinskii-Kosterlitz-Thouless (BKT) type [63], finite-size effects are only logarithmically small. Therefore, measuring the transition point numerically by physical observables is very tricky and inaccurate, so we employ a combination of methods. Only in the full thermodynamic limit, the charge gap increases from zero, the global compressibility goes to zero, the entanglement entropy drops from infinity to a finite value, and the fidelity susceptibility becomes extremely sharp at the transition point. The superfluid density ρ_s can be obtained using DMRG from the second-order response $[E_0(\theta) - E_0(0)]/\theta^2$ of the ground-state energy E_0 to a twist angle θ [64]. The response ρ_s is finite and increasing for small $\mathcal{J}_0[K]$, which shows that the system is indeed in a superfluid phase for this part of the phase diagram. The increase of ρ_s with effective hopping $\mathcal{J}_0[K]$ in Fig. 3(a) is not surprising since for smaller $\mathcal{J}_0[K]$ the hopping of type-a bosons is blocked by a changing occupation of type b, and vice versa. However, for larger $\mathcal{J}_0[K]$, a maximum and sudden drop to $\rho_s \to 0$ as $\mathcal{J}_0[K] \to 1$ signals a quantum phase transition to the well-established Mott state in the undriven system [52,65].

To pinpoint the transition point, we consider the fidelity susceptibility $\chi_F(\bar{x}) = -2 \ln F(x_1, x_2)/\delta^2$, which is defined via the overlap of ground states $F(x_1, x_2) = \langle \psi_0(x_1) | \psi_0(x_2) \rangle$ with $\delta = |x_1 - x_2|$ and $\bar{x} = (x_1 + x_2)/2$ for two close values x_1 and x_2 of the parameter $\mathcal{J}_0[K]$. A peak in χ_F is a clear signal of a quantum phase transition [66,67], which occurs at $\mathcal{J}_0[K]_c = 0.624(6)$. In addition, the entanglement entropy $\mathcal{S} = -\text{Tr}\rho_r \ln \rho_r$ is obtained from the partial trace of the reduced density matrix for half the system [68–70], which shows a distinct drop in the vicinity of the transition point. Using QMC, we find the compressibility $\kappa = \langle \hat{\mathcal{N}}^2 \rangle - \langle \hat{\mathcal{N}} \rangle^2$ for $L = 100$ sites at low temperatures, which vanishes in the deep Mott phase. The charge gap $\Delta_c = E_p + E_h - 2E_0$ is found by DMRG from the energies of systems with one additional particle E_p and one additional hole E_h relative to the ground state and becomes finite in the MI. After finite-size scaling analysis on $\mathcal{J}_0[K]_c$ by the level-spectroscopic technique discussed in Appendix C, we find that it matches well with the maxima in χ_F within error bars, so we use the latter to obtain the full phase diagram in Fig. 2(b).

At first sight, it is strange that the reduction in hopping $\mathcal{J}_0[K]$ can induce a SF state since normally weaker hopping makes the MI more stable. However, in this case, the density-dependent processes in Fig. 2 are responsible for a virtual exchange, which reduces the energy of an alternating density order *ababab*… to second order, $4J^2\mathcal{J}_0^2[K]/\bar{U}$ [14]. Therefore, by selectively tuning away those processes via periodic driving, the alternating order and the corresponding MI are actually *destabilized*, which in turn enables a SF for finite $\bar{U}$.

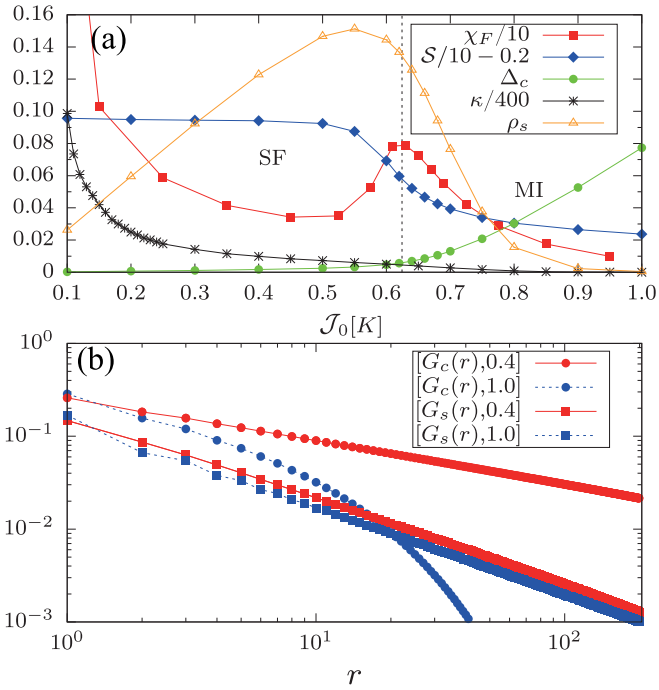

FIG. 3. Different observables at $J/\bar{U} = 0.4$. (a) Fidelity susceptibility χ_F and entanglement entropy $\mathcal{S}$ from iDMRG ($L = \infty$); charge gap Δ_c and superfluid density ρ_s from DMRG ($L = 100$); compressibility κ from QMC ($L = 100$). (b) Single-particle correlation $G_c(r) = \langle \hat{a}_0^\dagger \hat{a}_r \rangle$ (○) and density-hole-pair correlation $G_s(r) = \langle \hat{a}_0^\dagger \hat{b}_0 \hat{a}_r \hat{b}_r^\dagger \rangle$ (□) as a function of distance r relative to $L/4$ for $\mathcal{J}_0[K] = 0.4$ (solid line) and 1 (dashed line) obtained by DMRG ($L = 100$).

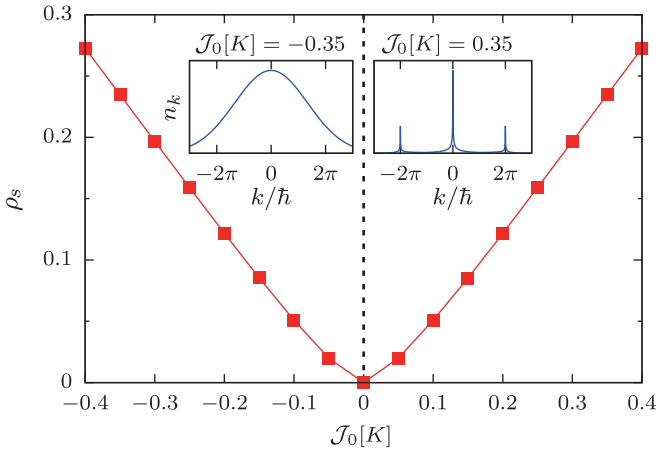

FIG. 4. Superfluid density ρ_s per site calculated by DMRG with $L = 100$ at $J = \bar{U}$. Inset: Momentum distribution n_k^b at $\mathcal{J}_0[K] = \pm 0.35$, which is normalized by its maximal value.

For $\mathcal{J}_0[K] = 0$, the system has no a-b-density correlations, which leads to the degeneracy discussed above.

It is instructive to analyze the characteristic correlation functions for the different phases as shown in Fig. 3(b) for $J = 0.4\bar{U}$. The single-particle correlation $G_c(r) = \langle \hat{a}_0^\dagger \hat{a}_r \rangle$ shows a typical power-law decay in the SF phase, $\mathcal{J}_0[K] = 0.4 < \mathcal{J}_0[K]_c$, while an exponential decay is a signature of a MI for $\mathcal{J}_0[K] = 1 > \mathcal{J}_0[K]_c$. The particle-hole-pair correlation $G_s(r) = \langle \hat{a}_0^\dagger \hat{b}_0 \hat{a}_r \hat{b}_r^\dagger \rangle$, on the other hand, shows a slow power-law decay in either phase.

C. Floquet-induced gauge-dressed superfluidity

We now turn to negative effective hopping $\mathcal{J}_0[K] < 0$. The corresponding phase diagram and the superfluid density are shown in Figs. 2(b) and 4, respectively. At first sight, the results look perfectly symmetric around $\mathcal{J}_0[K] = 0$, which would suggest that negative hopping has the same effect as positive hopping. However, the underlying states for positive and negative values are quite different, which becomes clear by looking at the signature of the momentum distribution (MD) n_k^b defined by

$$n_k^b = |w(k)|^2 \sum_{l,l'=1}^{L} \exp[ik(l-l')/\hbar] \langle \hat{b}_l^\dagger \hat{b}_{l'} \rangle, \tag{25}$$

as a function of momentum k, where $w(k)$ stands for the Fourier transformation of the Wannier function in a 1D optical lattice with lattice spacing equal to one [71]. As shown in the inset of Fig. 4, the MD shows an interference pattern with sharp peaks at $k = 0$ (modulo 2π) for positive values $\mathcal{J}_0[K] = 0.35$, which originates from the phase coherence of bosons in the normal SF. However, in the region $\mathcal{J}_0[K] < 0$, no sharp interference pattern is observed.

Both the symmetry in ρ_s and the difference in the MD interference pattern can be explained by a gauge transformation which defines new quasiparticles of type β, $\hat{\beta}_l = \hat{b}_l \exp(i\pi \hat{n}_l^a)$, and analogous for type α. We see that the hopping terms in Eqs. (21)–(23) can then be written as

$$\begin{aligned} \hat{J}_l^b \hat{b}_l^\dagger \hat{b}_{l+1} &= J\left(\frac{1+\mathcal{J}_0[K]}{2} + \frac{1-\mathcal{J}_0[K]}{2} e^{i\pi(\hat{n}_l^a + \hat{n}_{l+1}^a)}\right) \hat{b}_l^\dagger \hat{b}_{l+1} \\ &= J\left(\frac{1+\mathcal{J}_0[K]}{2} e^{i\pi(\hat{n}_l^a + \hat{n}_{l+1}^a)} + \frac{1-\mathcal{J}_0[K]}{2}\right) \hat{\beta}_l^\dagger \hat{\beta}_{l+1}, \end{aligned} \tag{26}$$

and likewise for $\hat{J}_l^a \hat{a}_l^\dagger \hat{a}_{l+1}$. Since the densities are not affected, $\hat{n}_l^{a/b} = \hat{n}_l^{\alpha/\beta}$, a change of sign $\mathcal{J}_0[K] \to -\mathcal{J}_0[K]$ is therefore equivalent to a transformation $\hat{b}_l \to \hat{\beta}_l$ and $\hat{a}_l \to \hat{\alpha}_l$ in Eq. (26). Accordingly, the energies and phase transition lines are identical for positive and negative $\mathcal{J}_0[K]$, but the superfluid density for the negative sign corresponds to a response of gauge-paired particles $\hat{\alpha}$, $\hat{\beta}$ and is therefore called a *gauge-dressed SF* with a different MD, as shown in the inset of Fig. 3. The transition to such an exotic condensed density can also be captured by a Gutzwiller mean-field argument, which is discussed in Appendix D. Note that the symmetry transformation to new gauge-paired particles in Eq. (26) is independent of the dimensionality and geometry of the lattice.

Thus, the gauge-dressed SF is characterized by a lattice gauge $\exp(i\pi \hat{n}_l^a)$ provided by one species (type a) which couples to the hopping of the other species (type b), and vice versa. As can be seen from Eq. (26), the gauge-dressed hopping becomes dominant in the strongly driven region $\mathcal{J}_0[K] < 0$, resulting in a superfluid response from gauge-dressed particles. The quantum phase transition to a MI is analogous to an ordinary SF and happens at exactly the same critical value of $J/\bar{U}$ in Fig. 2(b) as for corresponding positive $\mathcal{J}_0[K] > 0$ since the gauge does not change the energy response to a twist angle θ. The gauge-dressed SF is therefore different from pair superfluidity, where correlated hopping is observed due to a strong coupling of the hopping directly to the density [32,72]. The so-called counterflow SF is another type of correlated hopping [13–15], where hopping of particles of one species is facilitated by holes of the opposite species. In contrast, in the new gauge-dressed SF, the hopping is facilitated by gauges $\exp(i\pi \hat{n}_l^a)$, which can also be viewed as particles that are their own antiparticles, analogous to a Majorana description.

For the experimental realization of these phases, several critical questions must be solved. First of all, accessing the steady state by adiabatic ramping of the driving amplitude from the ground state is only possible when no dense avoided level crossing of the Floquet quasienergy takes place. Our analysis of the quasienergy spectrum in Appendix E ensures that there are no critical avoided level crossings in the relevant parameter range. Second, a measurement can be affected by the unitary transformation into the effective Floquet basis, if the operators do not commute with the kick operator. For stroboscopic measurements at times of integer multiples of period $T = 2\pi/\omega$ that this effect is reduced by $J/\hbar\omega$ in the high-frequency limit. For a separate check of the predictions, we also performed real-time simulations for a small lattice $L = 6$, shown in Appendix F, which clearly show the stability of the effective Hamiltonian and the feasibility of real-time dynamic measurements on finite timescales and length scales.

V. CONCLUSION AND OUTLOOK

In conclusion, we proposed a setup of a 1D lattice with two species of hard-core bosons and time-periodically modulated fields, which can be described by density-dependent tunneling with an interesting quantum phase diagram. By controlling the driving amplitude, density-dependent hopping processes are selectively tuned away, which are responsible for an alternating density *a*-*b* order. This in turn leads to a transition from the MI to a SF at half filling, in contrast to the undriven case. By tuning away these terms completely at $\mathcal{J}_0[K] = 0$, a highly degenerate state is obtained corresponding to an exactly solvable model without *a*-*b* correlations. For many-body systems, the study of nearly degenerate points is a very active research area, e.g., in the context of frustrated models, spin ice, and spin liquids. Much theoretical activity is devoted to studying novel quantum states, which are dominated by the quantum fluctuations near degenerate points, but we are not aware of any such studies for driving-induced degeneracy. In this case, dynamical effects will likely dominate the quantum correlations, which opens an interesting research field beyond our current abilities. For even larger driving amplitudes, negative hopping parameters $\mathcal{J}_0[K] < 0$ lead to a new *gauge-dressed SF* with a type of pairing mechanism where an atom of one species and a gauge phase of the other are bound to contribute to a nonzero superfluidity. This gauge-dressed SF has different correlations from an ordinary SF, as shown in Fig. 3 for the momentum distribution. Nonetheless, an exact hidden transformation to the positive hopping case can be found.

ACKNOWLEDGMENTS

We thank Youjin Deng, Shaon Sahoo, Oliver Thomas, and Zhensheng Yuan for the useful discussion. This research was supported by the Special Foundation from NSFC for theoretical physics Research Program of China (Grant No. 11647165), the Nachwuchsring of the TU Kaiserslautern. In particular, we gratefully acknowledge the computing time granted by the John von Neumann Institute for Computing (NIC) and provided on the supercomputer JURECA at the Jülich Supercomputing Centre (JSC). S.E., A.P., and M.F. acknowledge support from the German Research Foundation (DFG) through SFB/TR185, Project No. 277625399. X.-F.Z. acknowledges funding from Projects No. 2018CDQYWL0047 and No. 2019CDJDWL0005 supported by the Fundamental Research Funds for the Central Universities, Grant No. cstc2018jcyjAX0399 by the Chongqing Natural Science Foundation, and from the National Science Foundation of China under Grants No. 11804034, No. 11874094, and No. 11847301.

APPENDIX A: KICK OPERATOR AND OBSERVABLE IN LABORATORY FRAME

The dynamics of the system is not only determined by the effective Hamiltonian, but also the kick operator. If one prepares the system in the ground state of the nondriven Hamiltonian, then adiabatically turning on the driving has the consequence that the ground state of the system will follow the instantaneous stroboscopic Floquet Hamiltonian [35]. Thus the time-evolving wave function consists of the ground state $|\psi_e\rangle$ of the effective Hamiltonian (15) and a phase factor from the kick operator $\hat{\mathcal{K}}(t)$, namely,

$$|\psi(t)\rangle = e^{-i\hat{\mathcal{K}}(t)}|\psi_e\rangle. \tag{A1}$$

We also calculated the kick operator up to first order:

$$\hat{\mathcal{K}}^{(0)}(t) = 0, \tag{A2}$$

$$\hat{\mathcal{K}}^{(1)}(t) = \frac{1}{i\hbar\omega}\sum_{n\neq 0}\frac{e^{in\omega t}}{n}\hat{H}_r^{(n)} \approx \frac{2\hat{H}_r^{(1)}\cos(\omega t)}{i\hbar\omega}. \tag{A3}$$

So we get $\hat{\mathcal{K}}(nT) = \hat{\mathcal{K}}^{(1)}(nT) = 2\hat{H}_r^{(1)}/i\hbar\omega$. The expectation value $\langle\hat{\mathcal{O}}\rangle$ of an observable $\hat{\mathcal{O}}$ then results in

$$\langle\psi(nT)|\hat{\mathcal{O}}|\psi(nT)\rangle = \left\langle e^{2\hat{H}_r^{(1)}/\hbar\omega}\hat{\mathcal{O}}e^{-2\hat{H}_r^{(1)}/\hbar\omega}\right\rangle_e, \tag{A4}$$

where $\langle\hat{Q}\rangle_e \equiv \langle\psi_e|\hat{Q}|\psi_e\rangle$.

Thus, the expectation value of an observable in the laboratory coincides with that of the dressed observable $\exp(2\hat{H}_r^{(1)}/\hbar\omega)\hat{\mathcal{O}}\exp(-2\hat{H}_r^{(1)}/\hbar\omega)$, which is determined by the effective Hamiltonian. As $J/\hbar\omega$ is small, we only need to keep the two lowest orders,

$$\langle\hat{\mathcal{O}}\rangle = \langle\hat{\mathcal{O}}\rangle_e - \frac{2J}{\hbar\omega}\left\langle\left(\sum_l\left\{\hat{a}_l^\dagger\mathcal{J}_1\left[K_U\left(\hat{n}_l^b - \hat{n}_{l+1}^b\right)\right]\hat{a}_{l+1}\right.\right.\right.$$
$$\left.\left.\left. + \hat{b}_l^\dagger\mathcal{J}_1\left[K_U\left(\hat{n}_l^a - \hat{n}_{l+1}^a\right)\right]\hat{b}_{l+1} + \text{H.c.}\right\}, \hat{\mathcal{O}}\right)\right\rangle_e, \tag{A5}$$

for the driven interaction case, or

$$\langle\hat{\mathcal{O}}\rangle = \langle\hat{\mathcal{O}}\rangle_e - \frac{2J}{\hbar\omega}\left\langle\left(\sum_l\left\{\hat{b}_l^\dagger\mathcal{J}_1\left[K_U\left(\hat{n}_l^a - \hat{n}_{l+1}^b\right)\right]\hat{a}_{l+1}\right.\right.\right.$$
$$\left.\left.\left. + \hat{a}_l^\dagger\mathcal{J}_1\left[K_U\left(\hat{n}_l^b - \hat{n}_{l+1}^a\right)\right]\hat{b}_{l+1} + \text{H.c.}\right\}, \hat{\mathcal{O}}\right)\right\rangle_e, \tag{A6}$$

for the driven Rabi case. As a concrete example, we take the expectation value of $\hat{a}_k^\dagger\hat{a}_q$ in the driven interaction case, which has been used for calculating the momentum distribution, $\langle\hat{a}_k^\dagger\hat{a}_q\rangle = \langle\hat{a}_k^\dagger\hat{a}_q\rangle_e + 2\mathcal{J}_1[K_U]\langle\hat{A}\rangle_e J/\hbar\omega$, with

$$\begin{aligned}\hat{A} = {} & \hat{D}_{k-1,k}^b\left(1-2\hat{n}_k^a\right)\hat{a}_{k-1}^\dagger\hat{a}_q - \hat{X}_{k-1,k}^b\hat{a}_k^\dagger\hat{a}_q \\ & + \hat{D}_{k,k+1}^b\left(1-2\hat{n}_k^a\right)\hat{a}_{k+1}^\dagger\hat{a}_q + \hat{X}_{k,k+1}^b\hat{a}_k^\dagger\hat{a}_q \\ & + \hat{D}_{q-1,q}^b\left(2\hat{n}_q^a-1\right)\hat{a}_k^\dagger\hat{a}_{q-1} + \hat{X}_{q-1,q}^b\hat{a}_k^\dagger\hat{a}_q \\ & + \hat{D}_{q,q+1}^b\left(2\hat{n}_q^a-1\right)\hat{a}_k^\dagger\hat{a}_{q+1} - \hat{X}_{q,q+1}^b\hat{a}_k^\dagger\hat{a}_q,\end{aligned} \tag{A7}$$

with $\hat{D}_{l_1,l_2}^b = \hat{n}_{l_1}^b - \hat{n}_{l_2}^b$ and $\hat{X}_{l_1,l_2}^b = \hat{b}_{l_1}^\dagger\hat{b}_{l_2} + \text{H.c.}$ We read off that the correction operator $\hat{A}$ includes finite local terms. Note that one can always reduce the effect of the correction by tuning the value of $J/\hbar\omega$. In the driven Rabi case, the calculation is similar and the correction could be diminished by decreasing $J/\hbar\omega$.

At last, the effective Hamiltonian and the kick operator calculated above are defined in the rotating frame, but we are interested in observables in the laboratory frame. The link between both frames is provided by the fact that the time-evolving operators $\hat{U}(t_2,t_1)$ in the laboratory frame and $\hat{U}_r(t_2,t_1)$ in the rotating frame are connected by a rotation transformation, namely, $\hat{U}(t_2,t_1) = \hat{V}(t_2)\hat{U}_r(t_2,t_1)\hat{V}^\dagger(t_1)$. In

this paper, we are only interested in the *stroboscopic* dynamics at the moment $t = nT$, so we conclude $\hat{U}(t_2, t_1) = \hat{U}_r(t_2, t_1)$ and any observable turns out to be the same in both frames.

APPENDIX B: INTEGRABLE POINT

For the effective Hamiltonian given by Eq. (21) in the main text, the hopping term of the hardcore species a consists of two parts, $\hat{\mathcal{H}}_a = -J\hat{\mathcal{H}}_a^{(1)} - J\mathcal{J}_0[K]\hat{\mathcal{H}}_a^{(2)} + \text{H.c.}$, where

$$\hat{\mathcal{H}}_a^{(1)} = \sum_{l=1}^{L} \hat{a}_l^\dagger \hat{a}_{l+1} \big[\hat{n}_l^b \hat{n}_{l+1}^b + \big(1-\hat{n}_l^b\big)\big(1-\hat{n}_{l+1}^b\big)\big],$$
$$\hat{\mathcal{H}}_a^{(2)} = \sum_{l=1}^{L} \hat{a}_l^\dagger \hat{a}_{l+1} \big[\hat{n}_l^b \big(1-\hat{n}_{l+1}^b\big) + \big(1-\hat{n}_l^b\big)\hat{n}_{l+1}^b\big]. \quad \text{(B1)}$$

Here we use the hardcore constraint $\hat{a}_l\hat{a}_l^\dagger + \hat{a}_l^\dagger\hat{a}_l = 1$. The second part depends on the $\mathcal{J}_0[K]$ modulated by the normalized driven amplitude, while the first one does not. Similarly, the hopping term of the species b reads $\hat{\mathcal{H}}_b = -J\hat{\mathcal{H}}_b^{(1)} - J\mathcal{J}_0[K]\hat{\mathcal{H}}_b^{(2)} + \text{H.c.}$, where

$$\hat{\mathcal{H}}_b^{(1)} = \sum_{l=1}^{L} \hat{b}_l^\dagger \hat{b}_{l+1} \big[\hat{n}_l^a \hat{n}_{l+1}^a + \big(1-\hat{n}_l^a\big)\big(1-\hat{n}_{l+1}^a\big)\big],$$
$$\hat{\mathcal{H}}_b^{(2)} = \sum_{l=1}^{L} \hat{b}_l^\dagger \hat{b}_{l+1} \big[\hat{n}_l^a \big(1-\hat{n}_{l+1}^a\big) + \big(1-\hat{n}_l^a\big)\hat{n}_{l+1}^a\big]. \quad \text{(B2)}$$

At zeros of the zeroth-order first-kind Bessel function, namely, $\mathcal{J}_0[K] = 0$, $\hat{\mathcal{H}}_a = -J\hat{\mathcal{H}}_a^{(1)} + \text{H.c.}$ and $\hat{\mathcal{H}}_b = -J\hat{\mathcal{H}}_b^{(1)} + \text{H.c.}$ On the l site, we can define the number operators of the single a (a), single b (b), hole (h), and ab pair (p), respectively, namely,

$$\hat{\mathcal{N}}_l^a = \hat{n}_l^a\big(1-\hat{n}_l^b\big), \quad \hat{\mathcal{N}}_l^b = \big(1-\hat{n}_l^a\big)\hat{n}_l^b,$$
$$\hat{\mathcal{N}}_l^h = \big(1-\hat{n}_l^a\big)\big(1-\hat{n}_l^b\big), \quad \hat{\mathcal{N}}_l^p = \hat{n}_l^a\hat{n}_l^b, \quad \text{(B3)}$$

and thus the total number operators naturally read

$$\hat{\mathcal{N}}_t^{a(b,h,p)} = \sum_{l=1}^{L} \hat{\mathcal{N}}_l^{a(b,h,p)}. \quad \text{(B4)}$$

Because $[\hat{\mathcal{H}}_{a(b,\bar{U})}, \hat{\mathcal{N}}_t^{a(b,h,p)}] = 0$, the total numbers of the single a, single b, hole, and ab pair are all conserved in any eigenstate of the Hamiltonian. Furthermore, hopping terms of the species a and b can be divided into four individual and equivalent exchanging processes, that is,

$$\hat{\mathcal{H}}_a = -J\sum_{l=1}^{L}\big(\hat{S}_l^{pb,+}\hat{S}_{l+1}^{pb,-} + \hat{S}_l^{ha,+}\hat{S}_{l+1}^{ha,-} + \text{H.c.}\big),$$
$$\hat{\mathcal{H}}_b = -J\sum_{l=1}^{L}\big(\hat{S}_l^{pa,+}\hat{S}_{l+1}^{pa,-} + \hat{S}_l^{hb,+}\hat{S}_{l+1}^{hb,-} + \text{H.c.}\big), \quad \text{(B5)}$$

where

$$\hat{S}_l^{pa,+} = (\hat{a}_l^\dagger\hat{b}_l^\dagger)\hat{a}_l, \quad \hat{S}_l^{hb,+} = (\hat{a}_l\hat{b}_l)\hat{a}_l^\dagger,$$
$$\hat{S}_l^{pb,+} = (\hat{a}_l^\dagger\hat{b}_l^\dagger)\hat{b}_l, \quad \hat{S}_l^{ha,+} = (\hat{a}_l\hat{b}_l)\hat{b}_l^\dagger,$$
$$\hat{S}_l^{pa,-} = \hat{a}_l^\dagger(\hat{a}_l\hat{b}_l), \quad \hat{S}_l^{hb,-} = \hat{a}_l(\hat{a}_l^\dagger\hat{b}_l^\dagger),$$
$$\hat{S}_l^{pb,-} = \hat{b}_l^\dagger(\hat{a}_l\hat{b}_l), \quad \hat{S}_l^{ha,-} = \hat{b}_l(\hat{a}_l^\dagger\hat{b}_l^\dagger). \quad \text{(B6)}$$

The natural basis of a configuration consists of the single a, single b, hole, and ab pair on the different sites. From each configuration, we can extract two subsequences: one s_{ab} is built up by single occupations and the other s_{ph} contains all holes and ab pairs. To suppose that we have an initial configuration with two subsequences, hopping processes preserve these two sequences if no exchanging happens at edges. For example, an initial configuration for $L = 4$ sites is $|a_1p_2b_3h_4\rangle$ with subsequences $s_{ab} = \{|a\rangle, |b\rangle\}$ and $s_{ph} = \{|p\rangle, |h\rangle\}$. We get a new configuration $|a_1b_2p_3h_4\rangle$ under the exchanging process between the ab pair on the site-2 and the single b on the site-3. However, the new configuration has the same subsequences $s_{ab} = \{|a\rangle, |b\rangle\}$ and $s_{ph} = \{|p\rangle, |h\rangle\}$. And thus we consider them as two hidden conserved quantities to distinguish degenerate states.

The Hilbert space with certain $\mathcal{N}_t^{a(b,h,p)}$ can be blocked into $C(\mathcal{N}_t^a + \mathcal{N}_t^b, \mathcal{N}_t^a)C(\mathcal{N}_t^p + \mathcal{N}_t^h, \mathcal{N}_t^p)$ subspaces with a binomial coefficient $C(n, k)$, where we do not need to distinguish either a from b or the vacuum from the ab pair. Furthermore, we find the structure of subspaces is invariant if we replace either a (b) by b (a) or replace the vacuum (ab pair) by the ab pair (vacuum), which maintains $\mathcal{N}_t^a + \mathcal{N}_t^b$ and $\mathcal{N}_t^p + \mathcal{N}_t^h$ unchanged. That means when $\bar{U} = 0$, the Hamiltonian has a larger hidden symmetry, $D = Z_2^L$. Therefore, let us play a trick of preserving the hidden symmetry $\mathcal{D}$ as an inner one and regrouping four states: both a and b belong to the group "spin-down $\downarrow$," while both the vacuum and ab pair belong to the group "spin-up $\uparrow$," and the Hamiltonian becomes

$$\hat{\mathcal{H}}_a + \hat{\mathcal{H}}_b = \mathbb{I}_{\mathcal{D}} \otimes \hat{\mathcal{H}}_r, \quad \text{(B7)}$$

where $\hat{\mathcal{H}}_r = -J\sum_{l=1}^{L}(\hat{S}_l^+\hat{S}_{l+1}^- + \text{H.c.})$ and $\hat{S}_l^{+(-)}$ is the flip-up (-down) operator of the normal spin-1/2.

Usually, the on-site interacting term with finite $\bar{U}$ breaks exchanging symmetry $\mathcal{D}$, where the vacuum is inequivalent to the ab pair. However, the symmetry can be recovered in the case of the integer-1 filling, $\sum_{l=1}^{L}(\hat{n}_l^a + \hat{n}_l^b) = L$, where

$$\hat{\mathcal{H}}_{\bar{U}} = \bar{U}\sum_{l=1}^{L}\hat{n}_l^a\hat{n}_l^b$$
$$= \frac{\bar{U}}{2}\sum_{l=1}^{L}\left[2\left(\hat{n}_l^a - \frac{1}{2}\right)\left(\hat{n}_l^b - \frac{1}{2}\right) + \frac{1}{2} + \hat{n}_l^a + \hat{n}_l^a - 1\right]$$
$$= \frac{\bar{U}}{2}\sum_{l=1}^{L}\left[2\left(\hat{n}_l^a - \frac{1}{2}\right)\left(\hat{n}_l^b - \frac{1}{2}\right) + \frac{1}{2}\right]. \quad \text{(B8)}$$

Both the vacuum and ab pair contribute $\bar{U}/2$, while neither a nor b has a contribution. And thus the $\bar{U}$ term can be considered as an effective external magnetic field applied to the redefined spin-1/2, and the effective Hamiltonian in the reduced Hilbert space reads

$$\hat{H}_e^{(0)} = \sum_{l=1}^{L}\left[-J(\hat{S}_l^+\hat{S}_{l+1}^- + \text{H.c.}) + \frac{\bar{U}}{2}\big(\hat{S}_l^z + 1/2\big)\right], \quad \text{(B9)}$$

where $\hat{S}_l^z = 2(\hat{n}_l^a - 1/2)(\hat{n}_l^b - 1/2)$. By using the common Jordan-Wigner transformation, it becomes an integrable model in the language of spinless Fermi. We know the ground-state energy is $-2J\sum_{l=1}^{\mathcal{N}_t^a+\mathcal{N}_t^b}\cos[l\pi/(L+1)] + (\bar{U}/2)(\mathcal{N}_t^p + \mathcal{N}_t^h)$ with degeneracy equal to 2^L. That means the ground state has a finite residual entropy of $\ln 2$.

When we consider exchanging processes at the edges (e.g., with the periodic or twisted boundary conditions), the situation becomes a bit complicated. From an initial configuration with certain s_{ab} and s_{ph}, under the exchanging processes at edges we certainly get a new configuration with the other s'_{ab} and s'_{ph}. We also take $L = 4$ as an example: the initial configuration $|a_1 p_2 b_3 h_4\rangle$ transits into $|h_1 p_2 b_3 a_4\rangle$ under the exchanging process between the single a on the site-1 and the hole on the site-4. At the same time, subsequences $s_{ab} = |ab\rangle$ and $s_{ph} = |ph\rangle$ change to $s'_{ab} = |ba\rangle$ and $s'_{ph} = |hp\rangle$. Therefore, we have groups of relevant Hilbert subspaces with a periodic boundary condition. In one group consisting of $\mathcal{N}_s$ subspaces, the hopping process between two Hilbert subspaces only happens at edges and provides a phase shift $Q_q = 2q\pi/\mathcal{N}_s$ after a renormalization group manipulation, where $q = 0, 1, 2, \ldots, \mathcal{N}_s - 1$. And thus the single-particle spectrum is equal to $e_{m,q} = -2J\cos[2m\pi/L + (\mathcal{N}_t^a + \mathcal{N}_t^b)\pi/L + Q_q/L]$.

In the following paragraphs, we will see the physical properties of the integrable point. Let us first have a look at the single-particle correlation function of the species a, namely,

$$\begin{aligned}\langle \hat{a}_l^\dagger \hat{a}_{l'}\rangle &= \langle \hat{a}_l^\dagger(\hat{b}_l\hat{b}_l^\dagger + \hat{b}_l^\dagger\hat{b}_l)\hat{a}_{l'}(\hat{b}_{l'}\hat{b}_{l'}^\dagger + \hat{b}_{l'}^\dagger\hat{b}_{l'})\rangle \\ &= \left\langle \left(\hat{S}_l^{va,-} + \hat{S}_l^{pb,+}\right)\left(\hat{S}_{l'}^{va,+} + \hat{S}_{l'}^{pb,-}\right)\right\rangle \\ &= \left\langle \hat{S}_l^{va,-}\hat{S}_{l'}^{va,+} + \hat{S}_l^{pb,+}\hat{S}_{l'}^{pb,-}\right\rangle,\end{aligned}$$

where both of the mixing terms $\langle \hat{S}_l^{va,-}\hat{S}_{l'}^{pb,-}\rangle$ and $\langle \hat{S}_l^{pb,+}\hat{S}_{l'}^{va,+}\rangle$ are missing because none of them holds the total number of the single a, single b, vacuum, and ab pair at the integrable point. When we choose balanced filling $\sum_{l=1}^{L}\hat{n}_l^a = \sum_{l=1}^{L}\hat{n}_l^b$, the possibilities of exchanging processes between the single a (b) and vacuum (ab pair) are always equal and thus the above single-particle correlation function becomes

$$\langle \hat{a}_l^\dagger \hat{a}_{l'}\rangle = \tfrac{1}{4}\langle \hat{S}_l^-\hat{S}_{l'}^+ + \hat{S}_l^+\hat{S}_{l'}^-\rangle_r = \tfrac{1}{2}\langle \hat{S}_l^+\hat{S}_{l'}^-\rangle_r,$$

where we use the relation $\langle \hat{S}_l^+\hat{S}_{l'}^-\rangle_r = \langle \hat{S}_l^-\hat{S}_{l'}^+\rangle_r$ because the effective Hamiltonian is a real matrix.

Next we investigate the superfluid density at the integrable point. We use the original definition of superfluid density (or "spin stiffness"), which is the second-order response to the twisted phase on the edge bond. To suppose the twisted angle is θ, the hopping terms in the Hamiltonian become

$$\begin{aligned}\hat{\mathcal{H}}_a(\theta) = &-J\sum_{l=1}^{L-1}\left(\hat{S}_l^{pb,+}\hat{S}_{l+1}^{pb,-} + \hat{S}_l^{va,+}\hat{S}_{l+1}^{va,-} + \text{H.c.}\right) \\ &- Je^{i\theta}\left(\hat{S}_L^{pb,+}\hat{S}_1^{pb,-} + \hat{S}_L^{va,-}\hat{S}_1^{va,+} + \text{H.c.}\right), \\ \hat{\mathcal{H}}_b(\theta) = &-J\sum_{l=1}^{L-1}\left(\hat{S}_l^{pa,+}\hat{S}_{l+1}^{pa,-} + \hat{S}_l^{vb,+}\hat{S}_{l+1}^{vb,-} + \text{H.c.}\right) \\ &- Je^{i\theta}\left(\hat{S}_L^{pa,+}\hat{S}_1^{pa,-} + \hat{S}_L^{vb,-}\hat{S}_1^{vb,+} + \text{H.c.}\right), \quad \text{(B10)}\end{aligned}$$

where the exchanging process between the single a (b) and ab pair carries a positive phase, while the one between the single a (b) and vacuum carries a negative phase. The hidden inner symmetry D disappears and thus the model cannot be mapped to the effective spin-1/2 XY model. The on-site interacting term is invariant. The ground-state energy with infinitesimal twisted angle $\theta \ll 1$ can be expanded in the vicinity of $\theta = 0$, namely,

$$E_g(\theta) = E_g(0) + \tfrac{1}{2}\rho_s\theta^2 + o(\theta^3), \quad \text{(B11)}$$

where the first-order term disappears because when $\theta = 0$, the system holds the time-reversal symmetry and has no residual "current."

In fact, we can prove that the energy response is equal to zero for the case of integer-1 filling. From the effective model, the ground state occurs when $\mathcal{N}_t^a + \mathcal{N}_t^b = \mathcal{N}_t^p + \mathcal{N}_t^h = L/2$. Therefore, $\mathcal{N}_t^p = \mathcal{N}_t^h = L/4$. We have $L/2$ relevant Hilbert subspace: $L/4$ subspaces are connected by the exchanging processes between single occupations on the site-1 and holes on the site-L carrying a twisted phase $\exp(i\theta)$, while the other $L/4$ subspaces are connected by ones between single occupations on the site-1 and pairs on the site-L carrying a twisted phase $\exp(-i\theta)$. As a result, the residual twist phase in this group is equal to zero under the gauge transformation. The ground state has no energy response to the twisted phase on the boundary. In other words, their superfluid densities are all zero.

APPENDIX C: FINITE-SIZE SCALING

Because of the logarithmic corrections, it is a challenge to derive the accurate position of the BKT-type transition point from the Mott-insulator to superfluid phase by the finite-size scaling of the charge gap at zero temperature or compressibility χ at low temperature. In Fig. 5, curves $L\Delta_c$ collapse to one for small $\mathcal{J}_0[K]$, which means the charge gap Δ_c scales like $1/L$ in the deep superfluid region. In the deep Mott-insulating region when $\mathcal{J}_0[K]$ is large, Δ_c remains finite in the thermodynamical limit. On the anticipated critical point $\mathcal{J}_0[K]_c = 0.624(6)$, we find that curves $L\Delta_c$ with different system sizes get close to each other slowly but have no level crossings. Similarly, at low temperature $\beta/\bar{U} = 2L$, the compressibility is convergent to finite value and zero in the deep superfluid and Mott-insulating regions, respectively. However, the turning points for the finite system are slowly approaching $\mathcal{J}_0[K]_c$.

Under the Jordan-Wigner transformation, our model can be mapped to a density-dependent hopping Fermi-Hubbard model. And thus with the help of operator analysis in the level-spectroscopic technique several decades ago [73], we can choose the level crossing of two representative excited states to be the quasicritical point for the finite system. In the superfluid region, the representative excitation is a particle or hole if you add in or remove an atom. Whereas in the Mott-insulting region the lowest excitation is a pair made up of a particle a together with a hole b, or vice versa. The former has a gap $\Delta_c^+ = E_p - E_0 + \bar{U}/2$ measured from the energy of the system where we put one more particle E_p relative to the ground-state energy E_0. The latter has a pseudospin gap $\Delta_s^0 = E_1 - E_0$ with the first-excitation energy E_1 in the

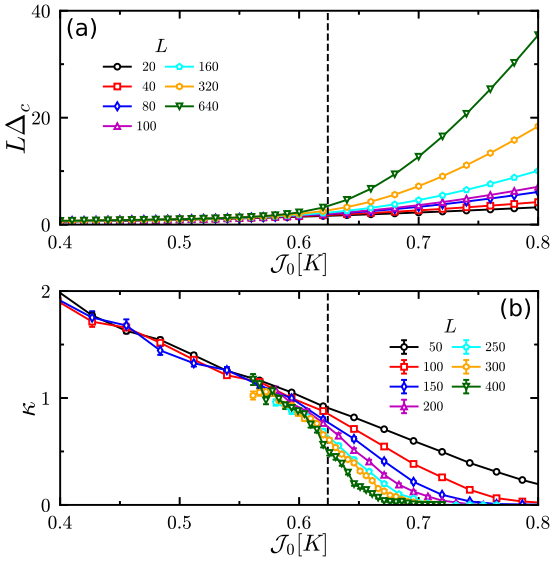

FIG. 5. Finite-size scaling of the (a) charge gap and (b) compressibility for the case of $J = 1$ and $\bar{U}/J = 0.4$. In DMRG, we choose the maximal truncation dimension $m = 4096$ for various system size $L = 20$ (black ○), 40 (red □), 80 (blue ⋄), 100 (magenta Δ), 160 (cyan ⬠), 320 (orange ⬡), and 640 (green ∇) with open boundary condition. In QMC, the inverse temperature $\beta/\bar{U} = 2L$ with $L = 50$ (black ○), 100 (red □), 150 (blue ⋄), 200 (magenta Δ), 250 (cyan ⬠), 300 (orange ⬡), and 400 (green ∇).

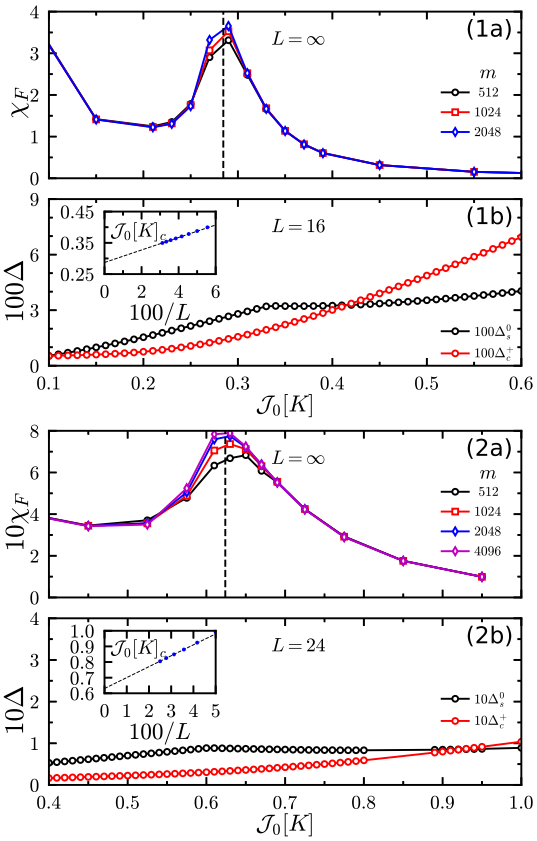

FIG. 6. Determinant on BKT-type transition points from the Mott-insulator to superfluid phase. (1a),(2a) The peaks of fidelity susceptibility measured from iDMRG indicate the transition points (1a) $\mathcal{J}_0[K]_c = 0.285(3)$ for $J/\bar{U} = 0.28$, and (2a) $\mathcal{J}_0[K]_c = 0.624(6)$ for $J/\bar{U} = 0.4$. (1b),(2b) We adopt the level-spectroscopic technique to achieve finite-size scaling. In the first step, we calculate excitation gaps $\Delta_c^+ = E_p - E_0 + \bar{U}/2$ (red hexagon) and $\Delta_s^0 = E_1 - E_0$ (black pentagon), where E_0 and E_1 are the ground state and the first-excited state in the Hilbert space $N^a = N^b = L/2$, respectively, and E_p is the lowest energy of the system where we add in one more particle relative to the ground state. Obviously, we find a level crossing between them called quasicritical points such as (1b) $\mathcal{J}_0[K]_{qc} = 0.415$ for $L = 16$ and $J/\bar{U} = 0.28$, and (2b) $\mathcal{J}_0[K]_{qc} = 0.924$ for $L = 24$ and $J/\bar{U} = 0.4$. In the second step, we plot the quasicritical points as a function of $1/L$ in the inset and find that they can be linearly extrapolated to the thermodynamical limit very well. We get the best extrapolation value $\mathcal{J}_0[K]_c = 0.287$ for $J/\bar{U} = 0.28$ and $\mathcal{J}_0[K]_c = 0.630$ for $J/\bar{U} = 0.4$, which remains consistent with the results from the iDMRG calculations in (1a) and (2a).

same Hilbert space $N^a = N^b = L/2$ for the ground state. In Figs. 6(1b) and 6(2b), the curves of two excitation gaps have level crossings for various finite system sizes. They scale very well as a linear function of $1/L$ in the insets and give us the position of BKT-type critical points in the thermodynamical limit. The extrapolation values also remain consistent with the investigation indicated by the peaks of fidelity susceptibility from iDMRG calculations.

APPENDIX D: GUTZWILLER MEAN FIELD

Here we exhibit the details of the Gutzwiller mean-field (GWMF) method. Because of $N_a = N_b = L/2$ and the hard-core constraint, the possibilities of the occupation by a pair or a hole, as well as that by a single atom a or b, are the same. Under the condition of normalization, we have an ansatz of the wave function in a uniform product matrix state, which reads

$$|\psi_g\rangle = \bigotimes_{l=1}^{L} \frac{1}{\sqrt{2}}[e^{i\phi_{0,0}} \sin\varphi|0,0\rangle + e^{i\phi_{0,1}} \cos\varphi|0,1\rangle + e^{i\phi_{1,0}} \cos\varphi|1,0\rangle + e^{i\phi_{1,1}} \sin\varphi|1,1\rangle], \quad \text{(D1)}$$

where $|n^a, n^b\rangle$ is for the local bases in a site, n^a and n^b are the numbers of species a and b, respectively, and φ and ϕ_{n^a,n^b} are the variational parameters. Thus, the average energy per site yields

$$e_g = \frac{1}{L}\langle\psi_g|\hat{H}_e^0|\psi_g\rangle = \frac{\bar{U}}{4}(1-\cos 2\varphi) - \frac{J}{2}(1-\cos^2 2\varphi)(1+\mathcal{J}_0[K]\cos\delta\phi), \quad \text{(D2)}$$

in which $\delta\phi = \phi_{0,0} - \phi_{1,0} - \phi_{0,1} + \phi_{1,1}$. Minimization of the energy gives the wave function of the ground state. Because $(1-\cos^2 2\varphi)$ is always larger than zero, the choice of the value of $\delta\phi$ in the ground-state wave function depends on the sign of $\mathcal{J}_0[K]$. In the region of $\mathcal{J}_0[K] > 0$, $\delta\phi = 0$, and $\cos 2\varphi = \bar{U}/[4J(1+|\mathcal{J}_0[K]|)]$, the condensed density $\rho_c^> = |\langle\hat{a}\rangle| = |\sin 2\varphi(1+e^{i\delta\phi})/4| = |\sin 2\varphi|/2 > 0$ when $J/\bar{U} > 1/4$, while in the region of $\mathcal{J}_0[K] < 0$, $|\mathcal{J}_0[K]| \ll 1$, and $J/\bar{U} > 1/4$, we get $\delta\phi = \pi$. The condensed density $\rho_c^> = |\langle\hat{a}\rangle| = |\sin 2\varphi(1+e^{i\delta\phi})/4| = 0$, while $\rho_c^< = |\hat{\alpha}\rangle| = |\hat{a}e^{i\pi\hat{n}_l^b}| = |\sin 2\varphi|/2 > 0$. That suggests a gauge-dressed superfluid phase in the region of $\mathcal{J}_0[K] < 0$.

APPENDIX E: AVOIDED LEVEL CROSSINGS

After a cloud of ultracold gases has been confined in the optical lattice and equilibrium in the ground state, relevant parameters (K_U, K_Ω, and $\bar{U}$) are adiabatically switched on in order to obtain the ground state of the effective Hamiltonian in the specified parameter regime. In previous studies, Eckardt *et al.* found that the request to the adiabatic modulation is not achievable if avoided level crossings between different Floquet bands emerge [74].

In this section, we investigate avoided level crossings in the quasienergy spectrum for a small system as a function of K and U, respectively. Besides the perturbative treatment in the last section, for the small system size, we can exactly diagonalize the general Floquet Hamiltonian $\hat{\mathcal{H}}(t) = \hat{H}(t) - i\hbar\partial/\partial t$, which obeys the general eigenequation

$$\hat{\mathcal{H}}(t)|\phi^\alpha(t)\rangle = \epsilon_\alpha|\phi^\alpha(t)\rangle, \tag{E1}$$

where the Floquet mode $|\phi^\alpha(t)\rangle$ is a many-body state instead of local Fock bases. The Floquet modes live in the Hilbert space of real dimensions $D_\mathcal{P}$. Because $|\phi^\alpha(t)\rangle = |\phi^\alpha(t+T)\rangle$, each Floquet mode can be expanded by Fourier modes,

$$\begin{aligned}|\phi^\alpha(t)\rangle &= \sum_{m=-\infty}^{+\infty} \exp(im\omega t)\left|\phi_m^\alpha\right\rangle \\ &= \sum_{m=-\infty}^{+\infty}\sum_{\{n_l^a n_l^b\}} \Lambda^{\alpha,m}_{\{n_l^a n_l^b\}} \exp(im\omega t)\left|\left\{n_l^a n_l^b\right\}\right\rangle \\ &= \sum_{m=-\infty}^{+\infty}\sum_{\{n_l^a n_l^b\}} \Lambda^{\alpha,m}_{\{n_l^a n_l^b\}} \left|m, \left\{n_l^a n_l^b\right\}\right\rangle. \end{aligned} \tag{E2}$$

The new bases $|m, \{n_l^a n_l^b\}\rangle$ satisfies the relation of super-orthogonalization,

$$\begin{aligned}&\left\langle\left\langle m, \left\{n_l^a n_l^b\right\}\middle| m', \left\{n_l^a n_l^b\right\}'\right\rangle\right\rangle \\ &= \frac{1}{T}\int_0^T dt\left\langle\left\{n_l^a n_l^b\right\}\middle|\left\{n_l^a n_l^b\right\}'\right\rangle e^{-i(m-m')\omega t} \\ &= \delta_{m,m'}\delta_{\{n_l^a n_l^b\},\{n_l^a n_l^b\}'}. \end{aligned} \tag{E3}$$

Equation (E1) can be interpreted as an eigenproblem defined in the enlarged Hilbert space $D_\mathcal{P} \otimes D_\mathcal{T}$ with number of frequencies $D_\mathcal{T} = \infty$. And thus we can also write the Floquet Hamiltonian in the enlarged Hilbert space,

$$\begin{aligned}\hat{\mathcal{H}}_{m;m'} &= \langle\langle m|\hat{\mathcal{H}}|m\rangle\rangle \\ &= \delta_{m,m'}(\hat{H}_T + \hat{H}_{\bar{U}}) + \frac{1}{2}(\delta_{m,m'+1} + \delta_{m,m'-1}) \\ &\quad\times\left[J_\Omega^0\sum_l(\hat{a}_l^\dagger\hat{b}_l + \text{H.c.}) + \delta U\sum_l \hat{n}_l^a\hat{n}_l^b\right]. \end{aligned} \tag{E4}$$

In principle, we get the full quasienergy spectrum by exactly diagonalizing the Floquet Hamiltonian. However, it is impossible to numerically handle an infinitely large matrix. In practice, because the spectrum has a repeating structure in energy axis, we only need to target $D_\mathcal{P}$ quasienergy levels in the vicinity of the zero-energy axis with $2N_D + 1$ cutting frequencies $m = -N_D, \ldots, N_D$. Then we use their translation invariant copies to cover the whole spectrum space. In this way, we can obtain the full quasienergy spectrum and find out the position of the avoided level crossings, and the valid parameter regime by investigating the position of the avoided level crossings, and thereby determine the valid regime which we can reach through the adiabatic switch-on.

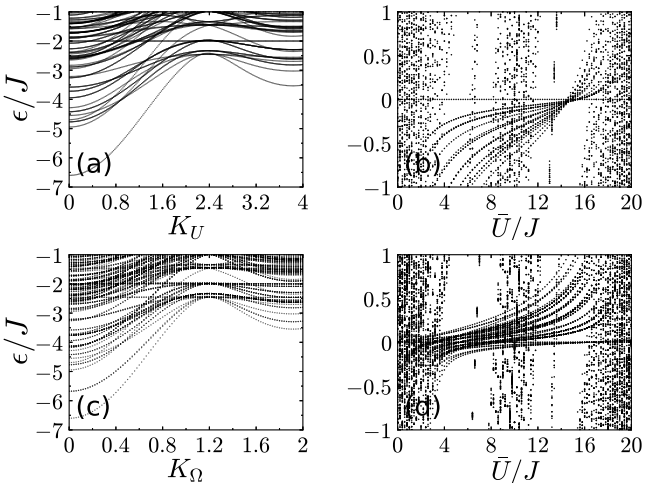

FIG. 7. Quasienergy spectrum of the Floquet Hamiltonian (E1) as a function of K_U, K_Ω, and $\bar{U}$, respectively. Here, $L = 6$, $\omega = 20$ and $N^a + N^b = 6$. (a),(b) $N^a = N^b = 3$. (a) $K_\Omega = 0$ and $\bar{U}/J = 1$, (b) $K_\Omega = 0$ and $K_U = 1$, (c) $K_U = 0$ and $\bar{U}/J = 1$, and (d) $K_U = 0$ and $K_\Omega = 1$.

In Fig. 7, we exhibit the quasienergy spectrum of the 6-sites as a function of K_U, K_Ω, and U, respectively. We choose the integer-1 filling $N^a + N^b = 6$ and relatively high-frequency $\omega = 20$ in general. In particular, $N^a = N^b = 3$ when $K_\Omega = 0$. When $\bar{U}/J = 1$ is fixed in Figs. 7(a) and 7(c), there is no problem in generating the adiabatic modulation of K_U or K_Ω. No extremely dense level avoided crossings are found. When $K_U = 1$ is fixed in Fig. 7(b) and $K_\Omega = 1$ in Fig. 7(d), we find several dense avoided level crossings occurring in the vicinity of $\bar{U}/J \approx 18$. This is in comparison with the ground-state phase diagram where the main interesting phases happen when $\bar{U}/J < 4$, and the avoided level crossings does not appear in this region. Thus, all the phases can be achieved by adiabatic modulation of $\bar{U}$.

APPENDIX F: REAL-TIME DYNAMICS

In the following, we check the real-time dynamics for a small system and answer the question of whether it is feasible to complete the preparation of the sample and the measurement before the thermalization sets in. To this end, we consider two steps for switching on K, i.e., K_U or K_Ω, and $\bar{U}$, respectively. At the first step, we initialize the system staying at the ground state of the nondriven model with a small on-site repulsion $\bar{U}^i$. Then, for $t > 0$, the amplitude of the time-periodic linearly polarized Raman laser beams is gradually switched on following a linear function of time t,

$$K(t) = \begin{cases} v_K t, & 0 < t \leqslant t_1 \\ K^f, & t > t_1, \end{cases} \tag{F1}$$

where the modulation lasts for the duration of $t_1 = n_{01}T$ until K reaches a desired value K^f so that the effective speed

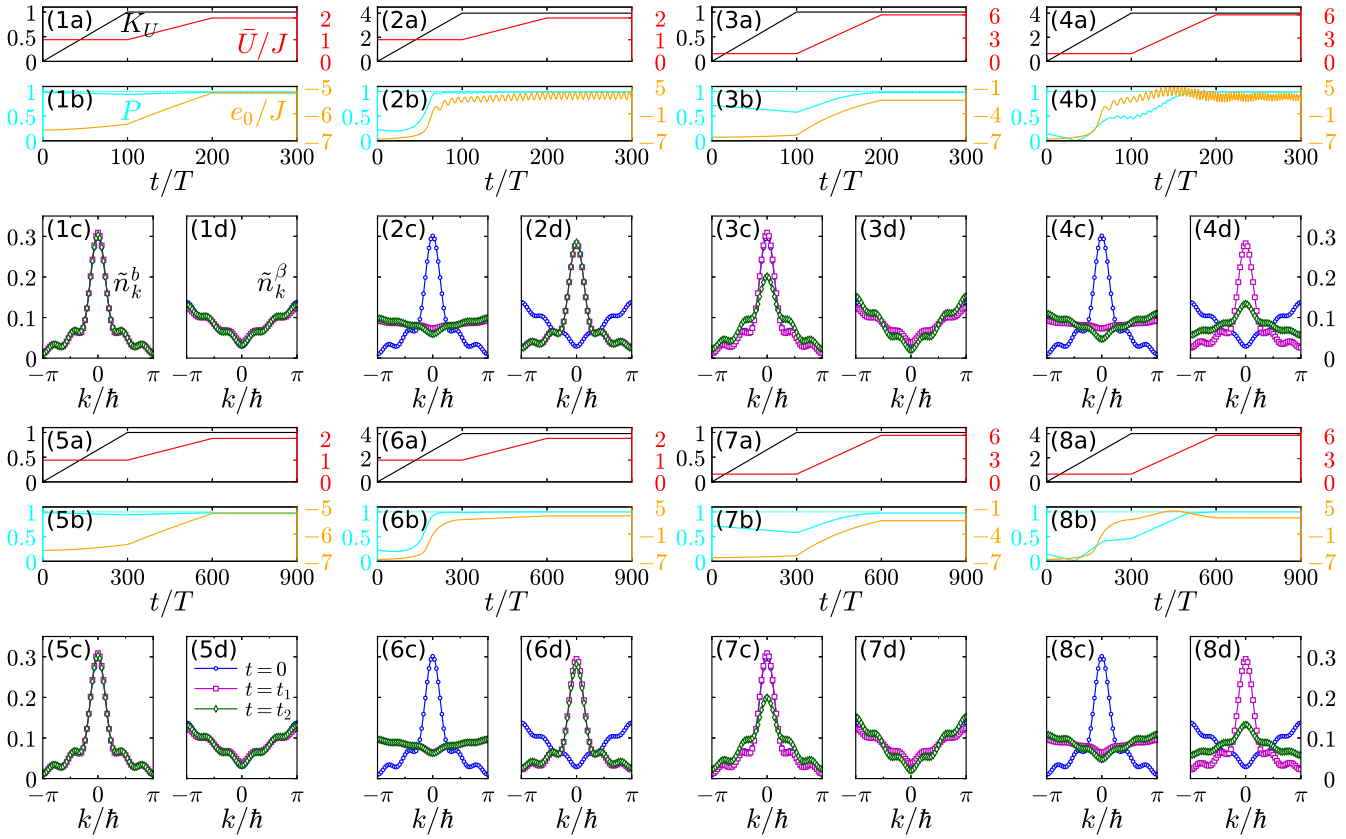

FIG. 8. Real-time dynamics for the model (7). Here we choose $L = 6$, $\hbar\omega/J = 20$, $K_\Omega = 0$, and $N^a = N^b = 3$. Initially, we prepare the system in the ground state of the nondriven model with $\bar{U}^i = 1$. K_U linearly grows until t_1 and persists as a working Rabi oscillation. At the moment t_1, we start to linearly increase $\bar{U}$ to a desired value $\bar{U}^f$ by t_2 and persist until the measurement. We consider two cases: (1)–(4) $t_1 = 100T$ and $t_2 = 200T$ for the fast switching-on, (5)–(8) $t_1 = 300T$ and $t_2 = 600T$ for the slow switching-on. For each case, we show the time-evolving behavior related to four different sets of parameters: (1) and (5) for $K_U^f = 1$ and $\bar{U}^f = 2$, (2) and (6) for $K_U^f = 4$ and $\bar{U}^f = 2$, (3) and (7) for $K_U^f = 1$ and $\bar{U}^f = 6$, and (4) and (8) for $K_U^f = 4$ and $\bar{U}^f = 6$. For each scheme, we show (a) modulated K_U (black lines) and $\bar{U}$ (red lines) as a function of time t/T, (b) time-evolving overlap P and energy e_0, and (c),(d) structure factors of $\tilde{n}_k^b$ and $\tilde{n}_k^\beta$ at the moment $t = 0$ (blue circles), $t = t_1$ (magenta squares), and $t = t_2$ (green diamonds), respectively.

$v_K = K^f/t_1$. It persists as a working Rabi oscillation before the measurement. In the second step, we turn on the on-site interaction gradually as a linear function of time t,

$$\bar{U}(t) = \begin{cases} \bar{U}^i, & 0 < t \leqslant t_1 \\ \bar{U}^i + v_{\bar{U}} t, & t_1 < t \leqslant t_2 \\ \bar{U}^f, & t > t_2, \end{cases} \tag{F2}$$

where the modulation lasts for the duration of $t_2 - t_1 = n_{12}T$ until the on-site interaction reaches a desired value $\bar{U}^f$ so the effective speed $v_{\bar{U}} = (\bar{U}^f - \bar{U}^i)/(t_2 - t_1)$.

After the modulation duration, we expect that the low-energy behavior of the system can be described by the effective Hamiltonian with the desired parameter values. Then the state should persist for a while in order to complete the measurement. Here we exploit the fourth-order Runge-Kutta method to solve a time-dependent Schrödinger equation and get the time-evolving wave function $|\psi(t)\rangle$. To understand how it is close to the desired one $|\psi_e\rangle$ (the ground state of the effective Hamiltonian with a desired parameter $\bar{U}^f$ and K^f), we measure a time-dependent overlap of them, namely,

$$P = |\langle\psi(t)|\psi_e\rangle|. \tag{F3}$$

Furthermore, we measure the time-dependent energy,

$$e_0(t) = \langle\psi(t)|\hat{H}_0|\psi(t)\rangle, \tag{F4}$$

and structure factors,

$$\tilde{n}_k^b = \frac{1}{L^2}\sum_{l,l'=1}^{L} \exp[ik(l-l')/\hbar]\langle\hat{b}_l^\dagger \hat{b}_{l'}\rangle, \tag{F5}$$

$$\tilde{n}_k^\beta = \frac{1}{L^2}\sum_{l,l'=1}^{L} \exp[ik(l-l')/\hbar]\langle\hat{\beta}_l^\dagger \hat{\beta}_{l'}\rangle, \tag{F6}$$

in comparison where $\hat{\beta}_l = \hat{b}_l \exp(i\pi\hat{n}_l^a)$ and $\hat{\beta}_l^\dagger = \hat{b}_l^\dagger \exp(-i\pi\hat{n}_l^a)$ are the annihilation and creation operators, respectively, for the gauge-dressed particles.

In Figs. 8 and 9, we systematically study the real-time dynamics for six sites in two cases of fast and slow switching-on. Although the middle process is complicated, the time-evolving overlap is close to 1 in company with an almost constant energy e_0 at the end of the modulations. That means that we can obtain the ground state of the effective Hamiltonian with the desired physical parameters following our scheme of sample preparation. In addition, slow

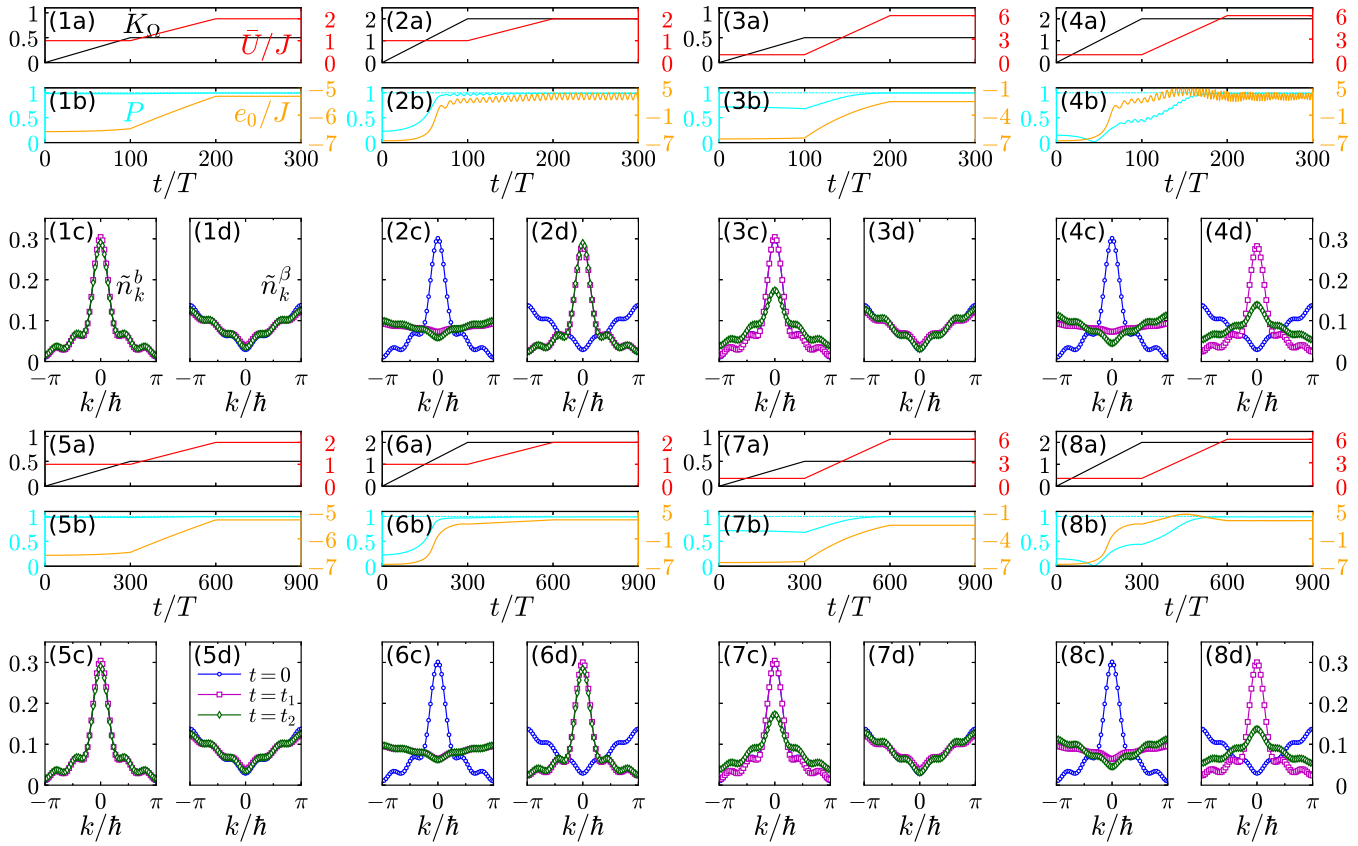

FIG. 9. Real-time dynamics for the model (11). Here we choose $L = 6$, $\hbar\omega/J = 20$, $K_U = 0$, and integer-1 filling $N^a + N^b = 6$. Initially, we prepare the system in the ground state of the nondriven model with $\bar{U}^i = 1$. K_Ω linearly grows until t_1 and persists as a working Rabi oscillation. At the moment t_1, we start to linearly increase $\bar{U}$ to a desired value $\bar{U}^f$ by t_2 and persist until the measurement. We consider two cases: (1)–(4) $t_1 = 100T$ and $t_2 = 200T$ for the fast switching-on, (5)–(8) $t_1 = 300T$ and $t_2 = 600T$ for the slow switching-on. For each case, we show the time-evolving behavior related to four different sets of parameters: (1) and (5) for $K_\Omega^f = 0.5$ and $\bar{U}^f = 2$, (2) and (6) for $K_\Omega^f = 2$ and $\bar{U}^f = 2$, (3) and (7) for $K_\Omega^f = 0.5$ and $\bar{U}^f = 6$, and (4) and (8) for $K_\Omega^f = 2$ and $\bar{U}^f = 6$. For each scheme, we show (a) modulated K_Ω (black lines) and $\bar{U}$ (red lines) as a function of time t/T, (b) time-evolving overlap P and energy e_0, and (c),(d) structure factors of $\tilde{n}_k^b$ and $\tilde{n}_k^\beta$ at the moment $t = 0$ (blue circles), t_1 (magenta squares), and t_2 (green diamonds), respectively.

switching-on always works better than the fast one and thus we suggest that the experimentalist needs to tune the parameters as slowly as possible before the thermalization happens.

[1] M. H. Anderson, J. R. Ensher, M. R. Matthews, C. E. Wieman, and E. A. Cornell, Observation of bose-einstein condensation in a dilute atomic vapor, Science **269**, 198 (1995).

[2] K. B. Davis, M. O. Mewes, M. R. Andrews, N. J. van Druten, D. S. Durfee, D. M. Kurn, and W. Ketterle, Bose-Einstein Condensation in a Gas of Sodium Atoms, Phys. Rev. Lett. **75**, 3969 (1995).

[3] M. P. A. Fisher, P. B. Weichman, G. Grinstein, and D. S. Fisher, Boson localization and the superfluid-insulator transition, Phys. Rev. B **40**, 546 (1989).

[4] D. Jaksch, C. Bruder, J. I. Cirac, C. W. Gardiner, and P. Zoller, Cold Bosonic Atoms in Optical Lattices, Phys. Rev. Lett. **81**, 3108 (1998).

[5] M. Greiner, O. Mandel, T. Esslinger, T. W. Hänsch, and I. Bloch, Quantum phase transition from a superfluid to a Mott insulator in a gas of ultracold atoms, Nature (London) **415**, 39 (2002).

[6] A. Hoffmann and A. Pelster, Visibility of cold atomic gases in optical lattices for finite temperatures, Phys. Rev. A **79**, 053623 (2009).

[7] C. Chin, R. Grimm, P. Julienne, and E. Tiesinga, Feshbach resonances in ultracold gases, Rev. Mod. Phys. **82**, 1225 (2010).

[8] K. Gross, C. P. Search, H. Pu, W. Zhang, and P. Meystre, Magnetism in a lattice of spinor Bose-Einstein condensates, Phys. Rev. A **66**, 033603 (2002).

[9] E. Demler and F. Zhou, Spinor Bosonic Atoms in Optical Lattices: Symmetry Breaking and Fractionalization, Phys. Rev. Lett. **88**, 163001 (2002).

[10] M. Mobarak and A. Pelster, Superfluid phases of spin-1 bosons in cubic optical lattice, Laser Phys. Lett. **10**, 115501 (2013).

[11] L.-M. Duan, E. Demler, and M. D. Lukin, Controlling Spin Exchange Interactions of Ultracold Atoms in Optical Lattices, Phys. Rev. Lett. **91**, 090402 (2003).

[12] W. Hofstetter, J. I. Cirac, P. Zoller, E. Demler, and M. D. Lukin, High-Temperature Superfluidity of Fermionic Atoms in Optical Lattices, Phys. Rev. Lett. **89**, 220407 (2002).

[13] A. B. Kuklov and B. V. Svistunov, Counterflow Superfluidity of Two-Species Ultracold Atoms in a Commensurate Optical Lattice, Phys. Rev. Lett. **90**, 100401 (2003).

[14] E. Altman, W. Hofstetter, E. Demler, and M. D. Lukin, Phase diagram of two-component bosons on an optical lattice, New J. Phys. **5**, 113 (2003).

[15] Y. Kuno, K. Kataoka, and I. Ichinose, Effective field theories for two-component repulsive bosons on lattice and their phase diagrams, Phys. Rev. B **87**, 014518 (2013).

[16] H.-N. Dai, B. Yang, A. Reingruber, H. Sun, X.-F. Xu, Y.-A. Chen, Z.-S. Yuan and J.-W. Pan, Four-body ring-exchange interactions and anyonic statistics within a minimal toric-code Hamiltonian, Nat. Phys. **13**, 1195 (2017).

[17] K. Mølmer, Bose Condensates and Fermi Gases at Zero Temperature, Phys. Rev. Lett. **80**, 1804 (1998).

[18] L. Viverit, C. J. Pethick, and H. Smith, Zero-temperature phase diagram of binary boson-fermion mixtures, Phys. Rev. A **61**, 053605 (2000).

[19] M. J. Bhaseen, M. Hohenadler, A. O. Silver, and B. D. Simons, Polaritons and Pairing Phenomena in Bose-Hubbard Mixtures, Phys. Rev. Lett. **102**, 135301 (2009).

[20] V. Bretin, S. Stock, Y. Seurin, and J. Dalibard, Fast Rotation of a Bose-Einstein Condensate, Phys. Rev. Lett. **92**, 050403 (2004).

[21] V. Schweikhard, I. Coddington, P. Engels, S. Tung, and E. A. Cornell, Vortex-Lattice Dynamics in Rotating Spinor Bose-Einstein Condensates, Phys. Rev. Lett. **93**, 210403 (2004).

[22] Y.-J. Lin, R. L. Compton, K. Jiménez-García, J. V. Porto, and I. B. Spielman, Synthetic magnetic fields for ultracold neutral atoms, Nature (London) **462**, 628 (2009).

[23] Y.-J. Lin, R. L. Compton, K. Jiménez-García, W. D. Phillips, J. V. Porto, and I. B. Spielman, A synthetic electric force acting on neutral atoms, Nat. Phys. **7**, 531 (2011).

[24] I. Vidanovic, A. Balaz, H. Al-Jibbouri, and A. Pelster, Nonlinear BEC dynamics induced by a harmonic modulation of the s-wave scattering length, Phys. Rev. A **84**, 013618 (2011).

[25] M. Di Liberto, C. E. Creffield, G. I. Japaridze, and C. Morais Smith, Quantum simulation of correlated-hopping models with fermions in optical lattices, Phys. Rev. A **89**, 013624 (2014).

[26] S. Greschner and L. Santos, Anyon Hubbard Model in One-Dimensional Optical Lattices, Phys. Rev. Lett. **115**, 053002 (2015).

[27] G. Tang, S. Eggert, and A. Pelster, Ground-state properties of anyons in a one-dimensional lattice, New J. Phys. **17**, 123016 (2015).

[28] C. Sträter, S. C. Srivastava, and A. Eckardt, Floquet Realization and Signatures of One-Dimensional Anyons in an Optical Lattice, Phys. Rev. Lett. **117**, 205303 (2016).

[29] T. Keilmann, S. Lanzmich, I. McCulloch, and M. Roncaglia, Statistically induced phase transitions and anyons in 1D optical lattices, Nat. Commun. **2**, 361 (2011).

[30] E. R. F. Ramos, E. A. L. Henn, J. A. Seman, M. A. Caracanhas, K. M. F. Magalhães, K. Helmerson, V. I. Yukalov, and V. S. Bagnato, Generation of non-ground-state Bose-Einstein condensates by modulating atomic interactions, Phys. Rev. A **78**, 063412 (2008).

[31] S. E. Pollack, D. Dries, R. G. Hulet, K. M. F. Magalhães, E. A. L. Henn, E. R. F. Ramos, M. A. Caracanhas, and V. S. Bagnato, Collective excitation of a Bose-Einstein condensate by modulation of the atomic scattering length, Phys. Rev. A **81**, 053627 (2010).

[32] A. Rapp, X. Deng, and L. Santos, Ultracold Lattice Gases with Periodically Modulated Interactions, Phys. Rev. Lett. **109**, 203005 (2012).

[33] T. Wang, X.-F. Zhang, F. E. A. dos Santos, S. Eggert, and A. Pelster, Tuning the quantum phase transition of bosons in optical lattices via periodic modulation of the s-wave scattering length, Phys. Rev. A **90**, 013633 (2014).

[34] S. Greschner, L. Santos, and D. Poletti, Exploring Unconventional Hubbard Models with Doubly Modulated Lattice Gases, Phys. Rev. Lett. **113**, 183002 (2014).

[35] A. Eckardt, Colloquium: Atomic quantum gases in periodically driven optical lattices, Rev. Mod. Phys. **89**, 011004 (2017).

[36] E. Arimondo, D. Ciampini, A. Eckardt, M. Holthaus, and O. Morsch, Kilohertz-driven bose einstein condensates in optical lattices, Adv. At. Mol. Opt. Phys. **61**, 515 (2012).

[37] F. Meinert, M. Mark, K. Lauber, A. Daley, and H.-C. Nägerl, Floquet Engineering of Correlated Tunneling in the Bose-Hubbard Model with Ultracold Atoms, Phys. Rev. Lett. **116**, 205301 (2016).

[38] J. Struck, C. Olschlager, R. Le Targat, P. Soltan-Panahi, A. Eckardt, M. Lewenstein, P. Windpassinger, and K. Sengstock, Quantum simulation of frustrated classical magnetism in triangular optical lattices, Science **333**, 996 (2011).

[39] J. Struck, C. Ölschläger, M. Weinberg, P. Hauke, J. Simonet, A. Eckardt, M. Lewenstein, K. Sengstock, and P. Windpassinger, Tunable Gauge Potential for Neutral and Spinless Particles in Driven Optical Lattices, Phys. Rev. Lett. **108**, 225304 (2012).

[40] P. Hauke, O. Tieleman, A. Celi, C. Ölschläger, J. Simonet, J. Struck, M. Weinberg, P. Windpassinger, K. Sengstock, M. Lewenstein, and A. Eckardt, Non-Abelian Gauge Fields and Topological Insulators in Shaken Optical Lattices, Phys. Rev. Lett. **109**, 145301 (2012).

[41] J. Struck, M. Weinberg, C. Ölschläger, P. Windpassinger, J. Simonet, K. Sengstock, R. Höppner, P. Hauke, A. Eckardt, M. Lewenstein *et al.*, Engineering Ising-XY spin-models in a triangular lattice using tunable artificial gauge fields, Nat. Phys. **9**, 738 (2013).

[42] M. Aidelsburger, M. Atala, S. Nascimbène, S. Trotzky, Y.-A. Chen, and I. Bloch, Experimental Realization of Strong Effective Magnetic Fields in an Optical Lattice, Phys. Rev. Lett. **107**, 255301 (2011).

[43] H. Lignier, C. Sias, D. Ciampini, Y. Singh, A. Zenesini, O. Morsch, and E. Arimondo, Dynamical Control of Matter-Wave Tunneling in Periodic Potentials, Phys. Rev. Lett. **99**, 220403 (2007).

[44] G. Jotzu, M. Messer, F. Görg, D. Greif, R. Desbuquois, and T. Esslinger, Creating State-Dependent Lattices for Ultracold Fermions by Magnetic Gradient Modulation, Phys. Rev. Lett. **115**, 073002 (2015).

[45] F. Görg, M. Messer, K. Sandholzer, G. Jotzu, R. Desbuquois, and T. Esslinger, Enhancement and sign change of magnetic correlations in a driven quantum many-body system, Nature (London) **553**, 481 (2018).

[46] A. Zenesini, H. Lignier, D. Ciampini, O. Morsch, and E. Arimondo, Coherent Control of Dressed Matter Waves, Phys. Rev. Lett. **102**, 100403 (2009).

[47] W. Zwerger, Mott-Hubbard transition of cold atoms in optical lattices, J. Opt. B: Quantum Semiclass. Opt. **5**, S9 (2003).
[48] A. Marte, T. Volz, J. Schuster, S. Dürr, G. Rempe, E. G. M. van Kempen, and B. J. Verhaar, Feshbach Resonances in Rubidium 87: Precision Measurement and Analysis, Phys. Rev. Lett. **89**, 283202 (2002).
[49] J. B. Naber, L. Torralbo-Campo, T. Hubert, and R. J. C. Spreeuw, Raman transitions between hyperfine clock states in a magnetic trap, Phys. Rev. A **94**, 013427 (2016).
[50] J. Sapriel, S. Francis, and B. Kelly, *Acousto-Optics* (Wiley, Chichester, NY, 1979).
[51] H. Eklund, A. Roos, and S. T. Eng, Rotation of laser beam polarization in acousto-optic devices, Opt. Quantum Electron. **7**, 73 (1975).
[52] E. H. Lieb and F. Y. Wu, Absence of Mott Transition in an Exact Solution of the Short-Range, One-Band Model in One Dimension, Phys. Rev. Lett. **20**, 1445 (1968).
[53] S. R. White, Density Matrix Formulation for Quantum Renormalization Groups, Phys. Rev. Lett. **69**, 2863 (1992).
[54] S. R. White, Density-matrix algorithms for quantum renormalization groups, Phys. Rev. B **48**, 10345 (1993).
[55] *Density-Matrix Renormalization*, edited by I. Peschel, X. Q. Wang, M. Kaulke, and K. Hallberg (Springer, Berlin, 1999).
[56] U. Schollwöck, The density-matrix renormalization group, Rev. Mod. Phys. **77**, 259 (2005).
[57] I. P. McCulloch, Infinite size density matrix renormalization group, revisited, arXiv:0804.2509.
[58] S. Hu, B. Normand, X. Wang, and L. Yu, Accurate determination of the Gaussian transition in spin-1 chains with single-ion anisotropy, Phys. Rev. B **84**, 220402(R) (2011).
[59] S. Hu, A. M. Turner, K. Penc, and F. Pollmann, Berry-Phase-Induced Dimerization in One-Dimensional Quadrupolar Systems, Phys. Rev. Lett. **113**, 027202 (2014).
[60] A. W. Sandvik, Stochastic series expansion method with operator-loop update, Phys. Rev. B **59**, R14157 (1999).
[61] O. F. Syljuåsen and A. W. Sandvik, Quantum Monte Carlo with directed loops, Phys. Rev. E **66**, 046701 (2002).
[62] K. Louis and C. Gros, Stochastic cluster series expansion for quantum spin systems, Phys. Rev. B **70**, 100410(R) (2004).
[63] T. D. Kühner and H. Monien, Phases of the one-dimensional Bose-Hubbard model, Phys. Rev. B **58**, R14741 (1998).
[64] R. Roth and K. Burnett, Superfluidity and interference pattern of ultracold bosons in optical lattices, Phys. Rev. A **67**, 031602(R) (2003).
[65] F. Essler, H. Frahm, F. Göhmann, A. Klümper, and V. Korepin, *The One-Dimensional Hubbard Model* (Cambridge University Press, Cambridge, 2005).
[66] W.-L. You, Y.-W. Li, and S.-J. Gu, Fidelity, dynamic structure factor, and susceptibility in critical phenomena, Phys. Rev. E **76**, 022101 (2007).
[67] L. C. Venuti and P. Zanardi, Quantum Critical Scaling of the Geometric Tensors, Phys. Rev. Lett. **99**, 095701 (2007).
[68] A. Osterloh, L. Amico, G. Falci, and R. Fazio, Scaling of entanglement close to a quantum phase transition, Nature (London) **416**, 608 (2002).
[69] L.-A. Wu, M. S. Sarandy, and D. A. Lidar, Quantum Phase Transitions and Bipartite Entanglement, Phys. Rev. Lett. **93**, 250404 (2004).
[70] N. Laflorencie, Quantum entanglement in condensed matter systems, Phys. Rep. **646**, 1 (2016).
[71] R. Walters, G. Cotugno, T. H. Johnson, S. R. Clark, and D. Jaksch, *Ab initio* derivation of Hubbard models for cold atoms in optical lattices, Phys. Rev. A **87**, 043613 (2013).
[72] K. P. Schmidt, J. Dorier, A. Läuchli, and F. Mila, Single-particle versus pair condensation of hard-core bosons with correlated hopping, Phys. Rev. B **74**, 174508 (2006).
[73] M. Nakamura, Tricritical behavior in the extended Hubbard chains, Phys. Rev. B **61**, 16377 (2000).
[74] A. Eckardt and M. Holthaus, Avoided-Level-Crossing Spectroscopy with Dressed Matter Waves, Phys. Rev. Lett. **101**, 245302 (2008).